*Supporting Information*

# Enhanced In Vitro Antiviral Activity of Hydroxychloroquine Ionic Liquids Against SARS-CoV-2

*FTIR spectra*

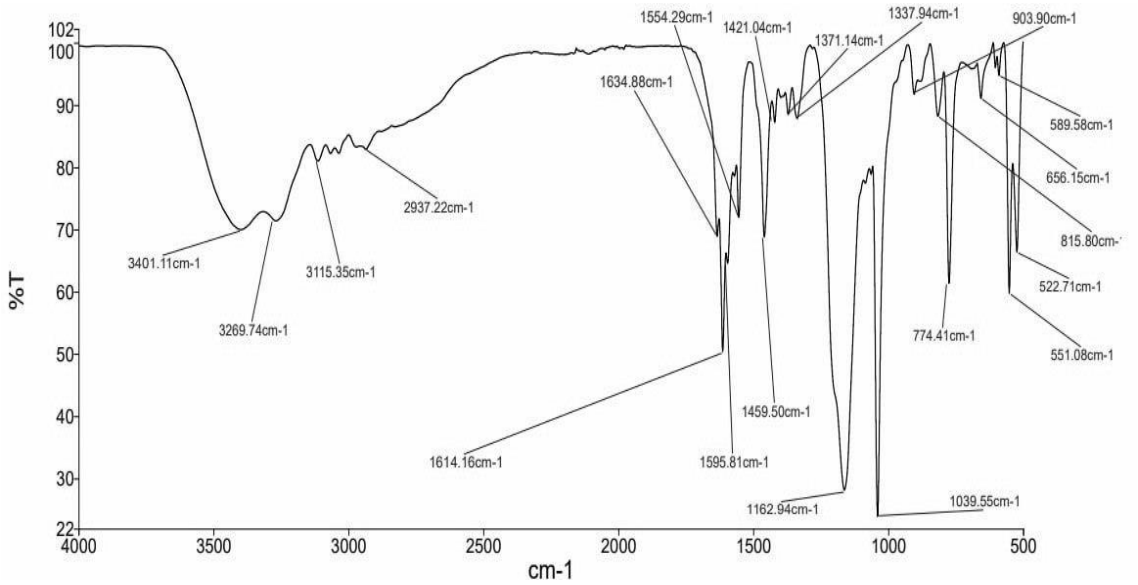


Figure S1. FTIR-ATR spectrum of $[HCQH_2][C_1SO_3]_2$.

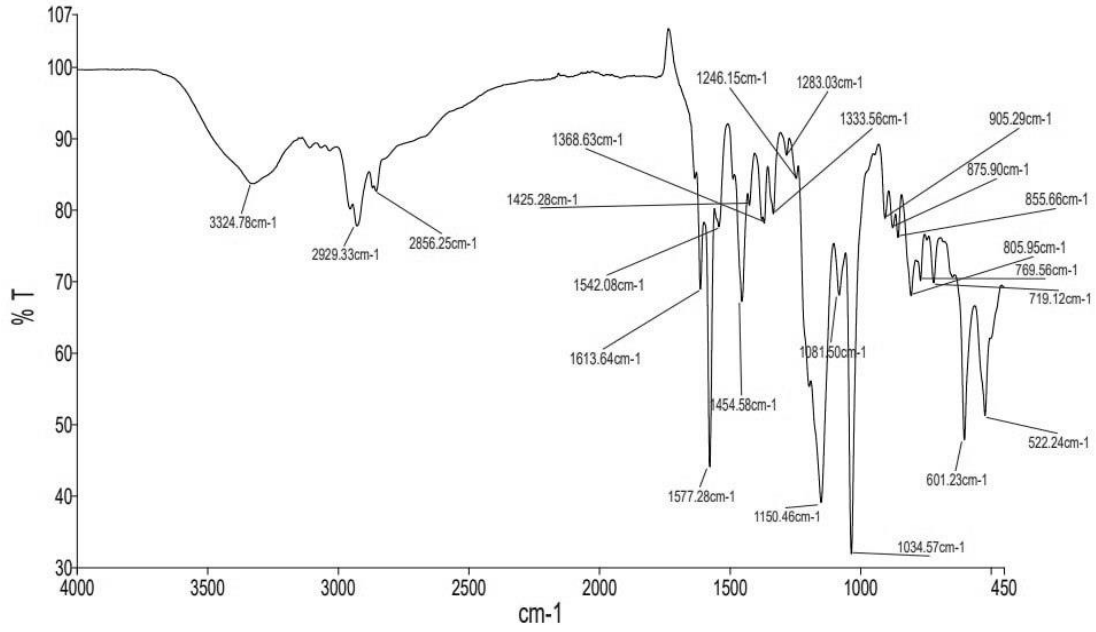


Figure S2. FTIR-ATR spectrum of $[HCQH_2][C_6SO_3]_2$.

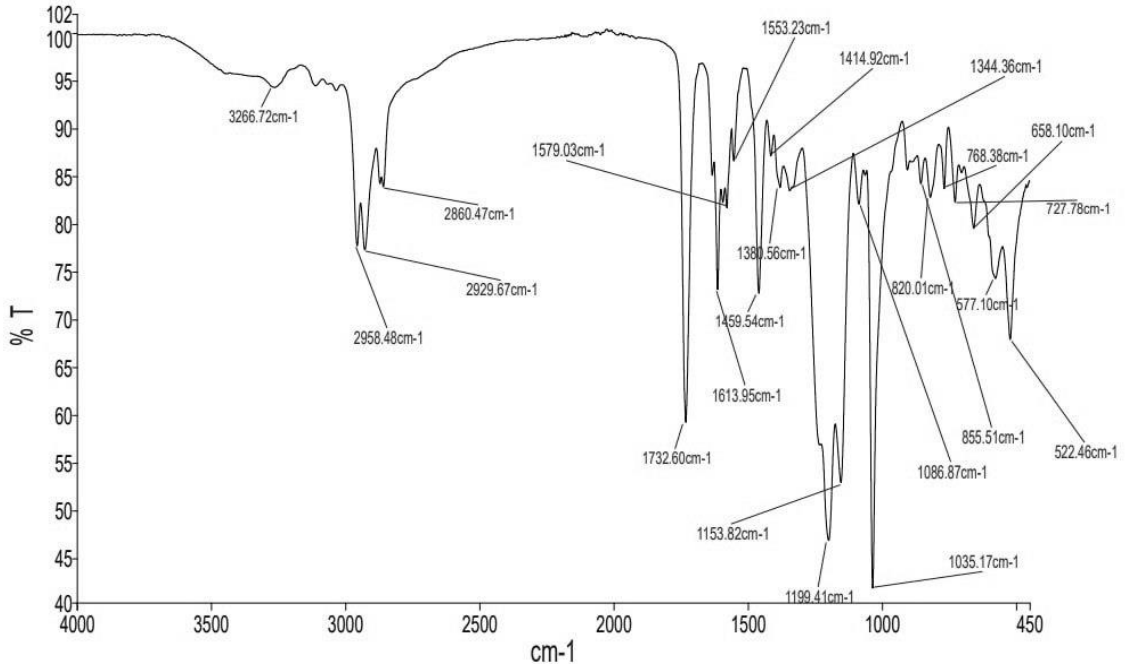


Figure S3. FTIR-ATR spectrum of $[HCQH_2][DocSO_3]_2$.

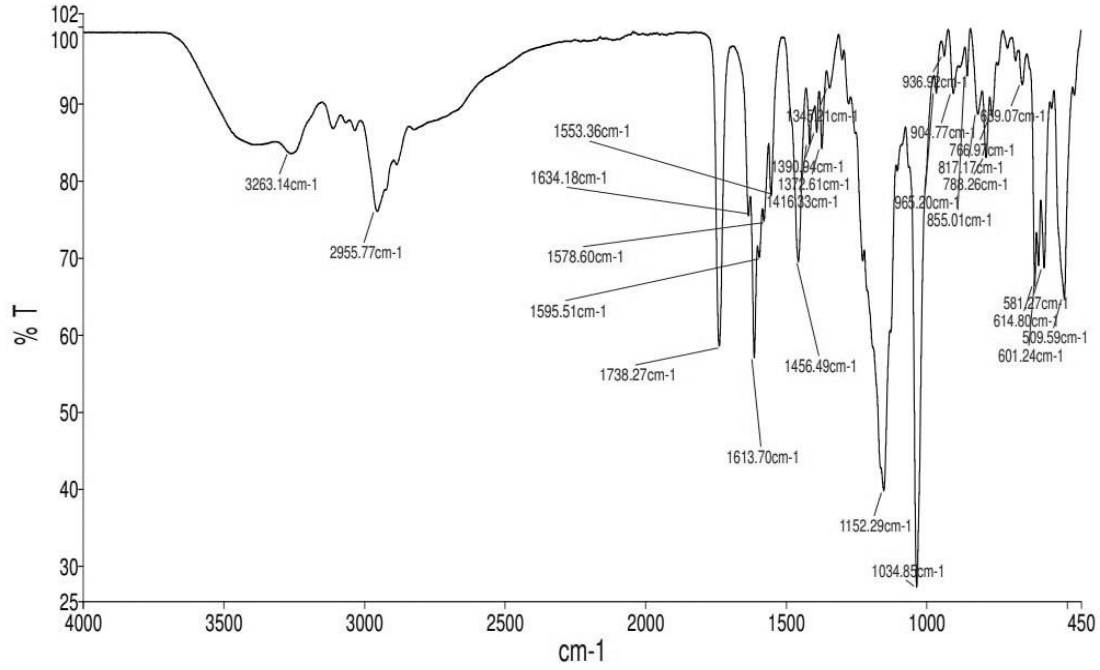


Figure S4. FTIR-ATR spectrum of $[HCQH_2][CampSO_3]_2$.

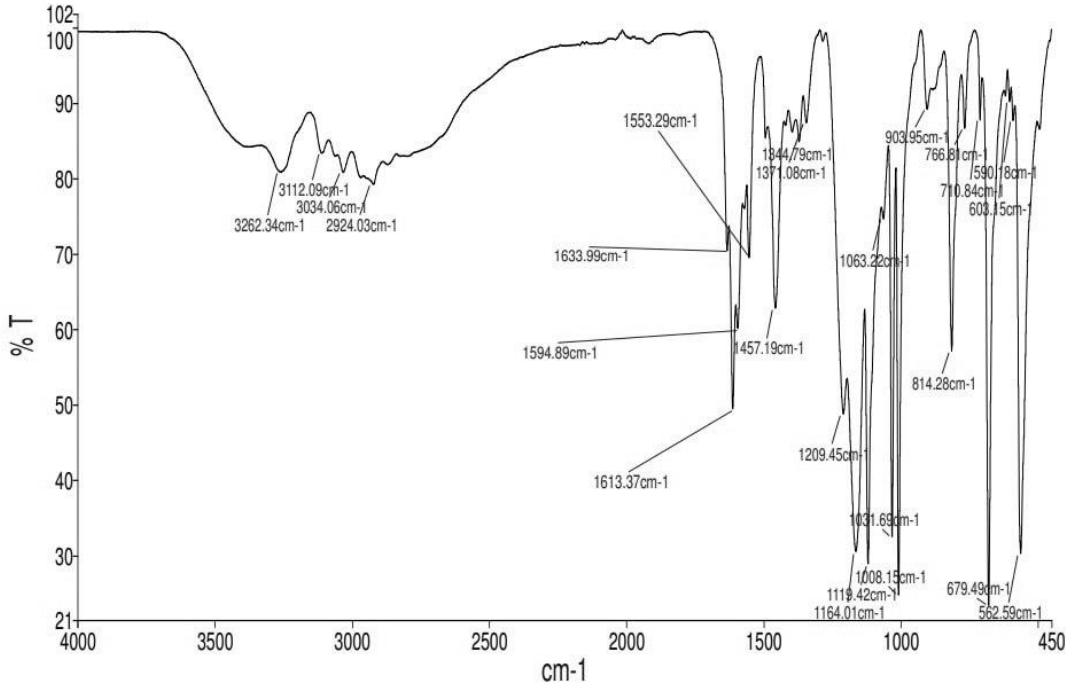


Figure S5. FTIR-ATR spectrum of [HCQH$_2$][*p*-TolSO$_3$]$_2$.

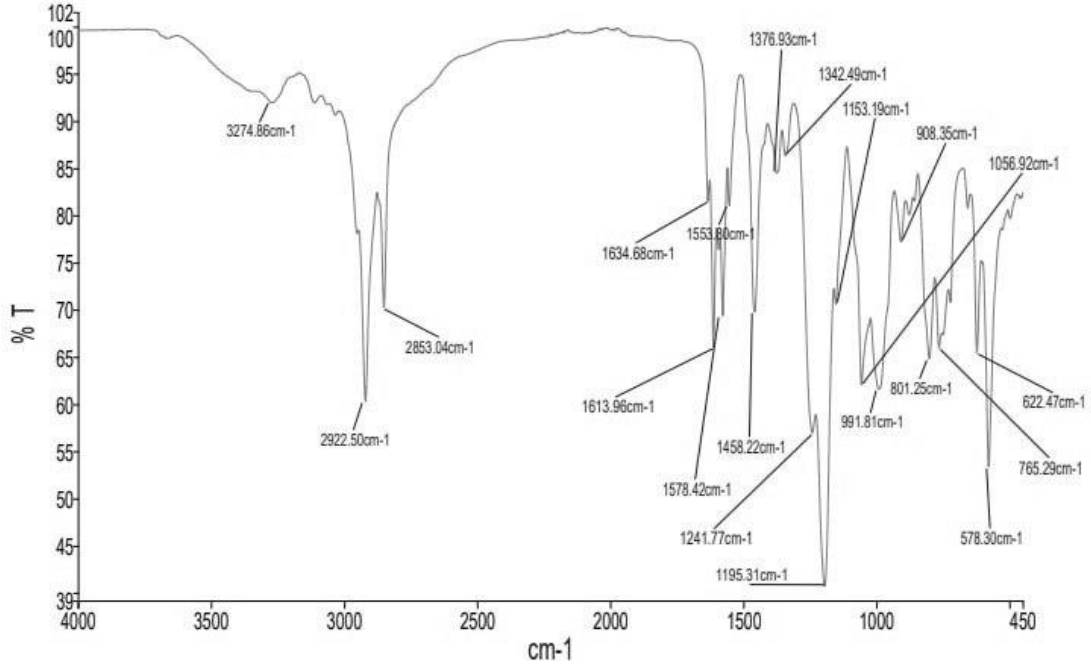


Figure S6. FTIR-ATR spectrum of [HCQH$_2$][C$_{12}$SO$_4$]$_2$.

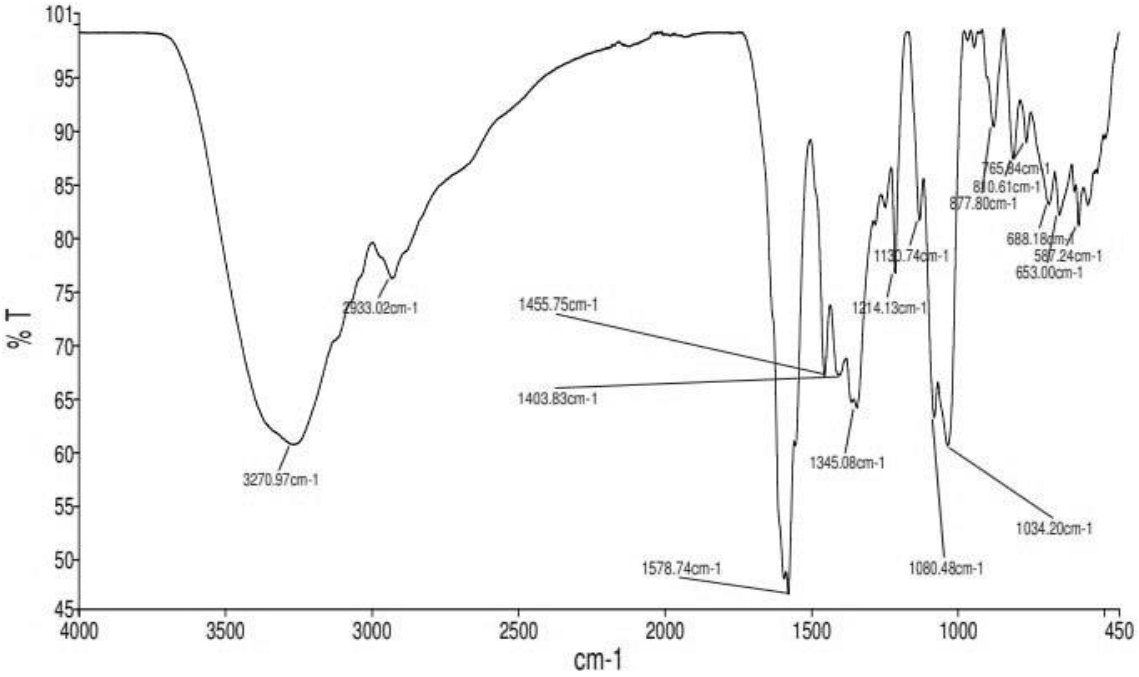


Figure S7. FTIR-ATR spectrum of $[HCQH_2][GlcCOO]_2$.

*NMR spectra*

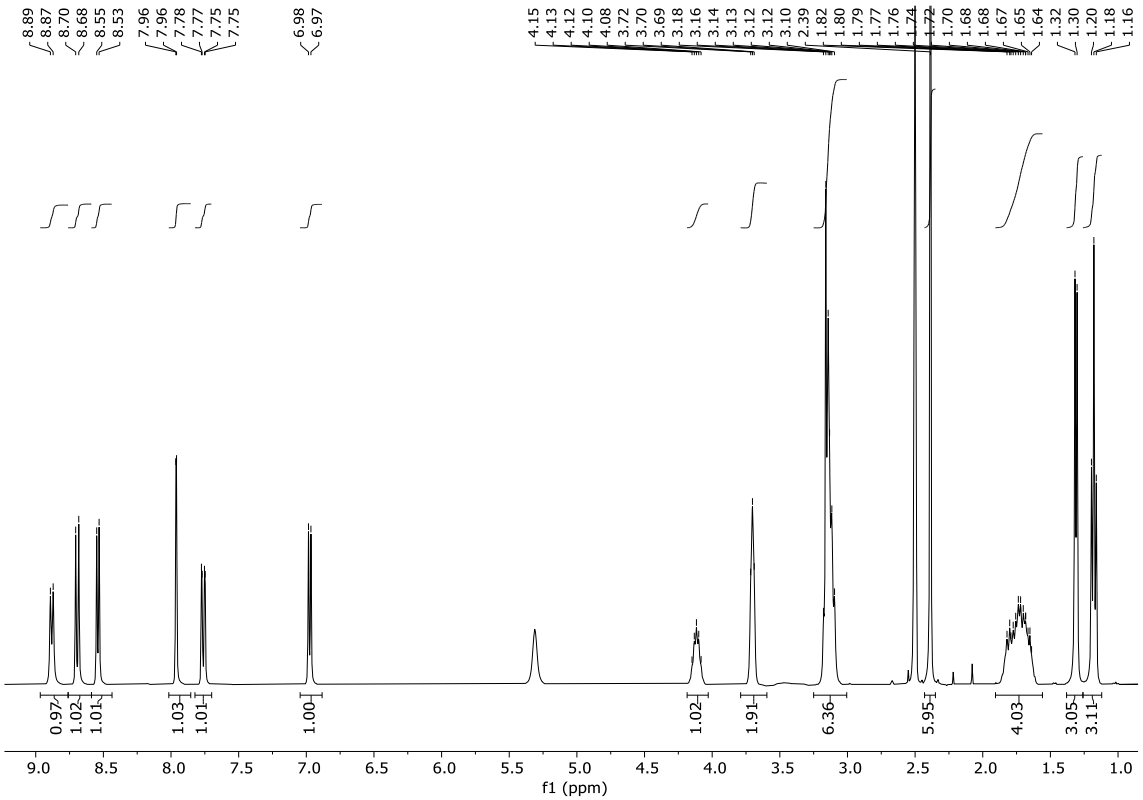


Figure S8. $^{1}$H NMR spectrum of $[HCQH_2][C_1SO_3]_2$ in DMSO-$d_6$.

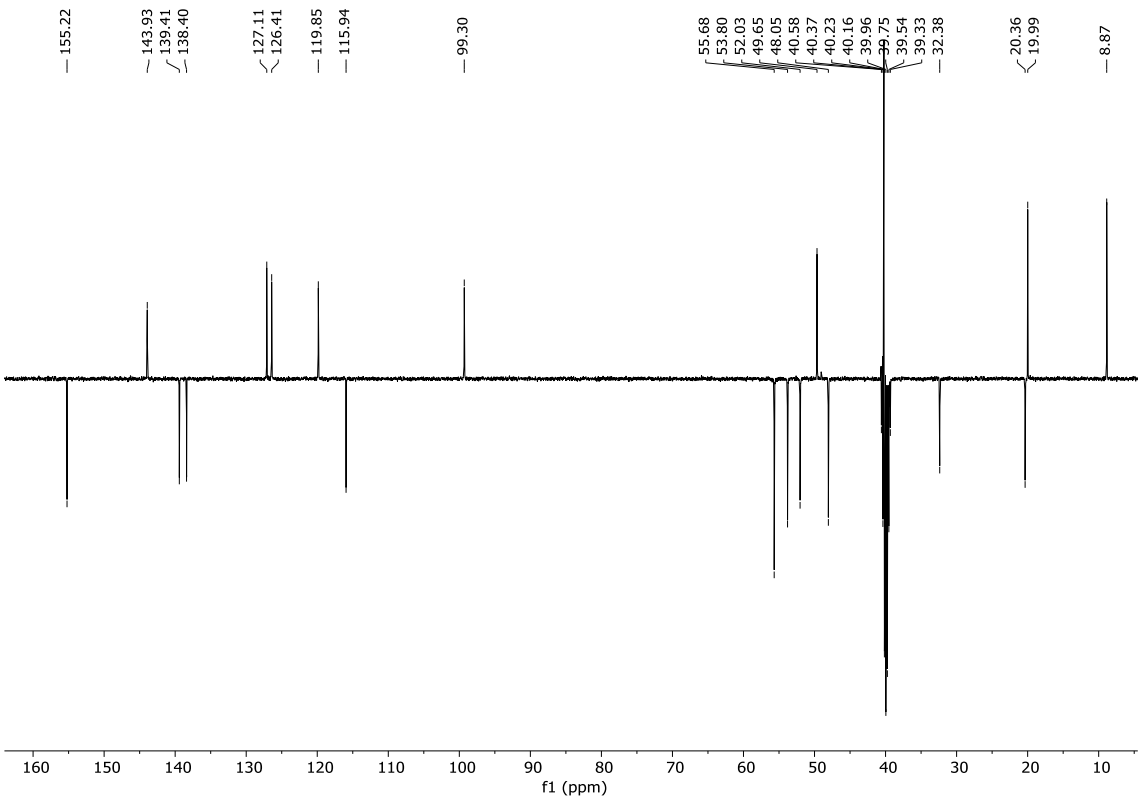


Figure S9. $^{13}$C APT NMR spectrum of $[HCQH_2][C_1SO_3]_2$ in DMSO-$d_6$.

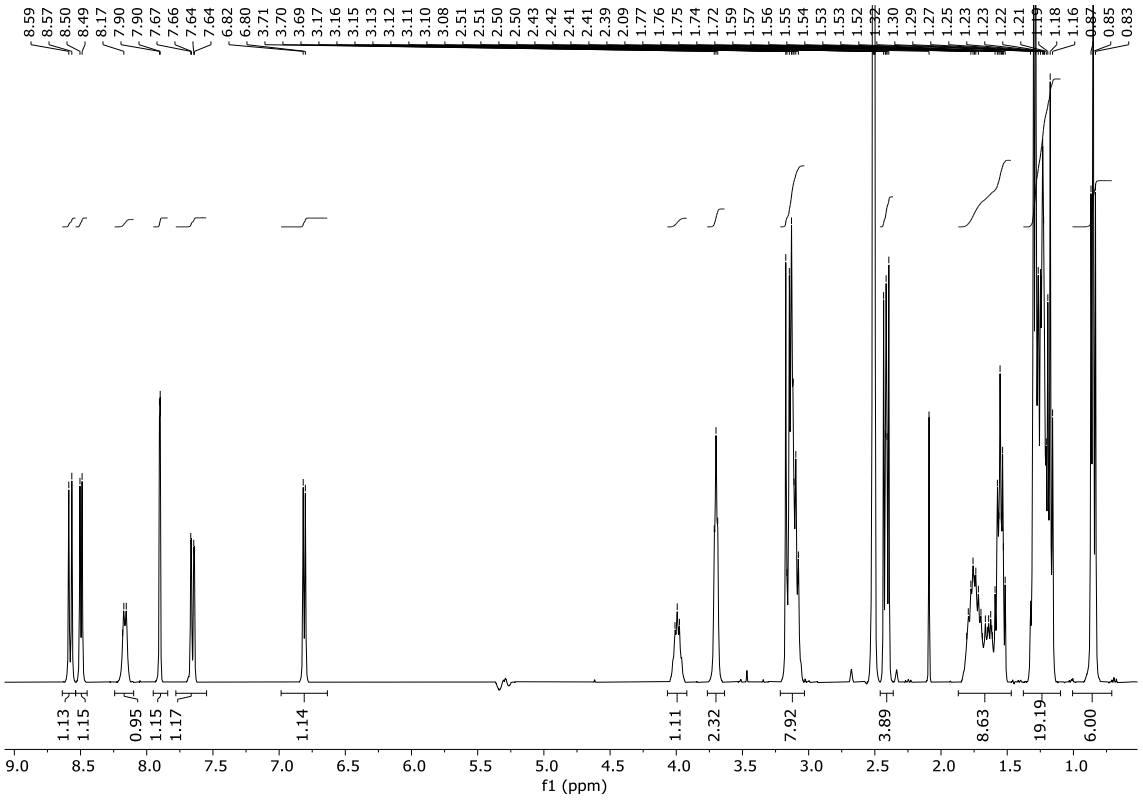


Figure S10. $^{1}H$ NMR spectrum of $[HCQH_2][C_6SO_3]_2$ in DMSO-$d_6$.

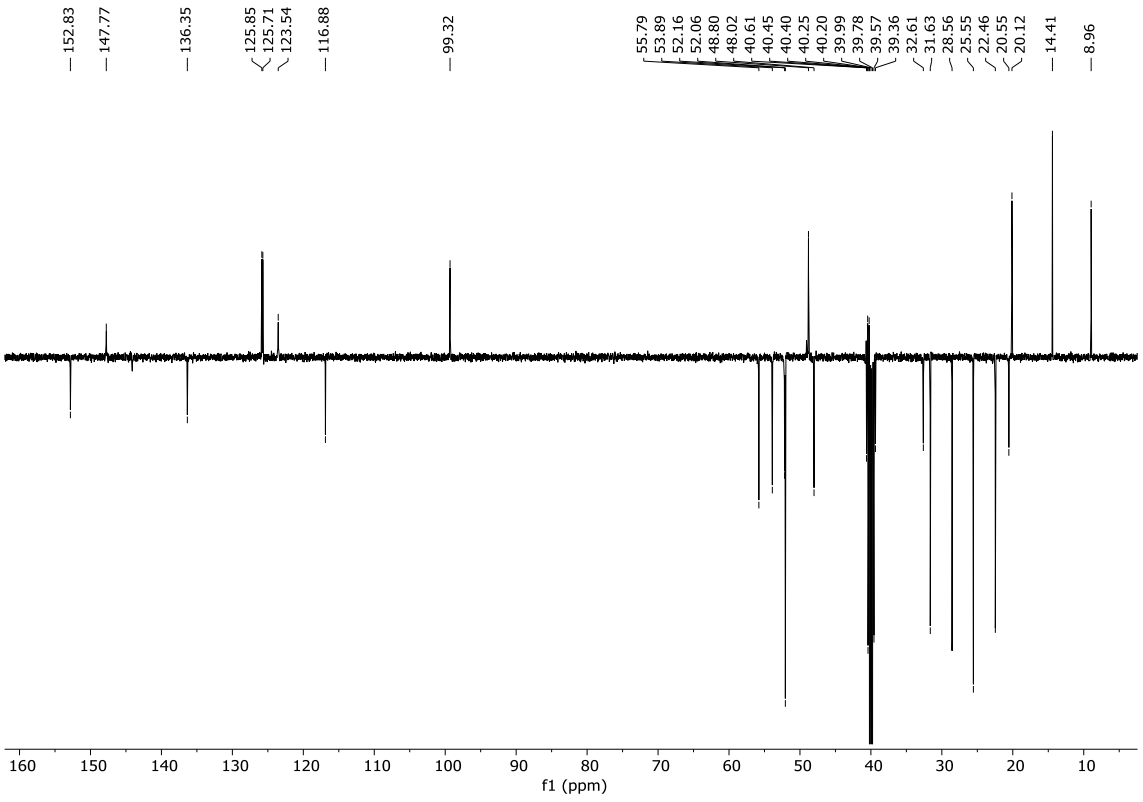


Figure S11. $^{13}C$ APT NMR spectrum of $[HCQH_2][C_6SO_3]_2$ in DMSO-$d_6$.

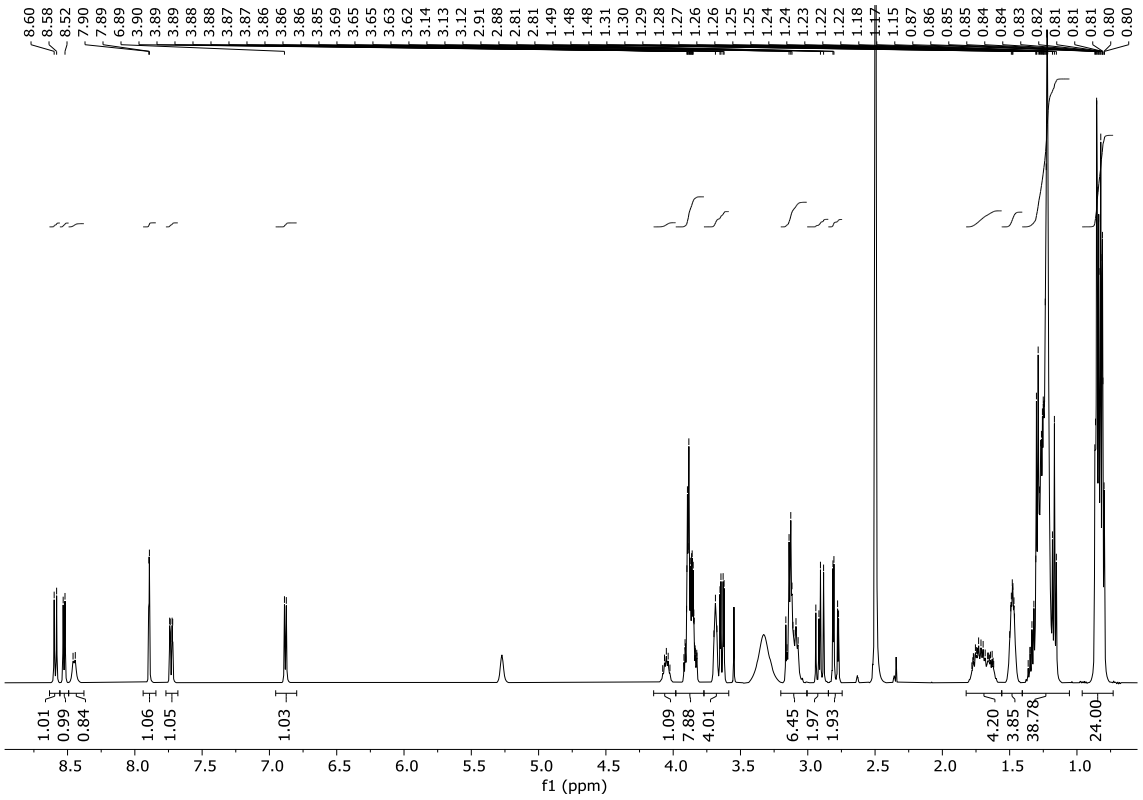


Figure S12. $^{1}H$ NMR spectrum of $[HCQH_2][DocSO_3]_2$ in DMSO-$d_6$.

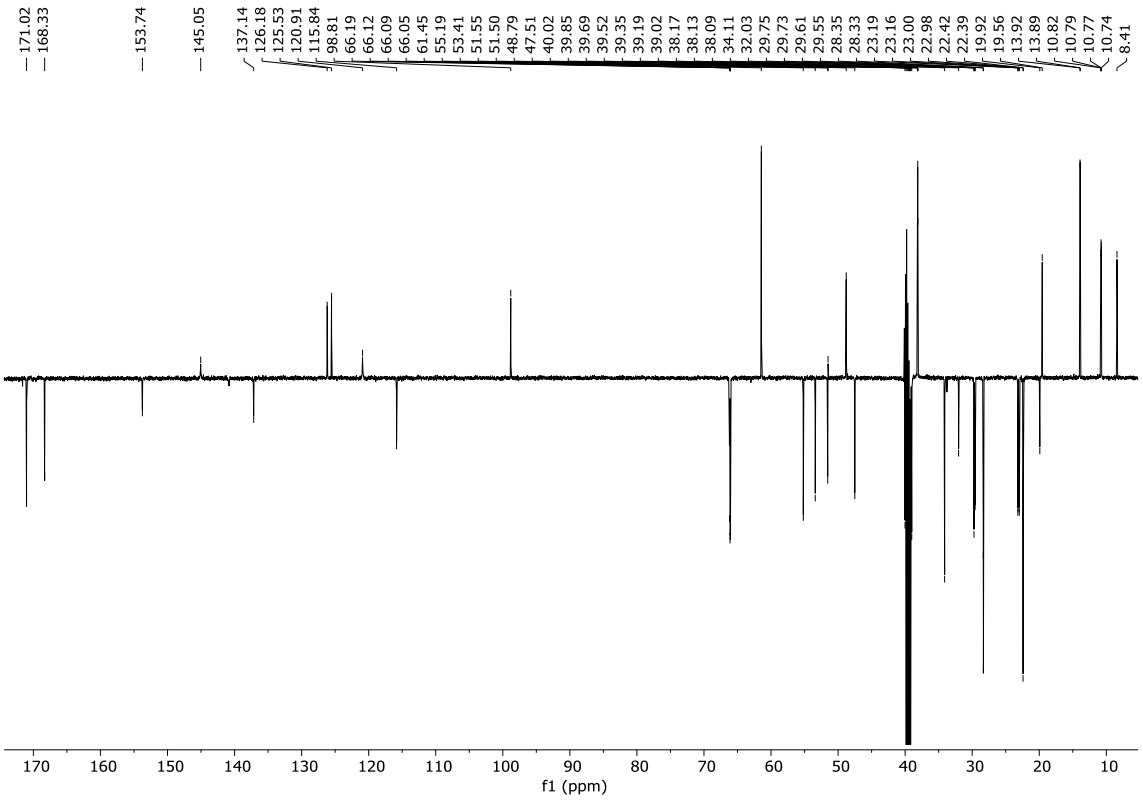


Figure S13. $^{13}C$ APT NMR spectrum of $[HCQH_2][DocSO_3]_2$ in DMSO-$d_6$.

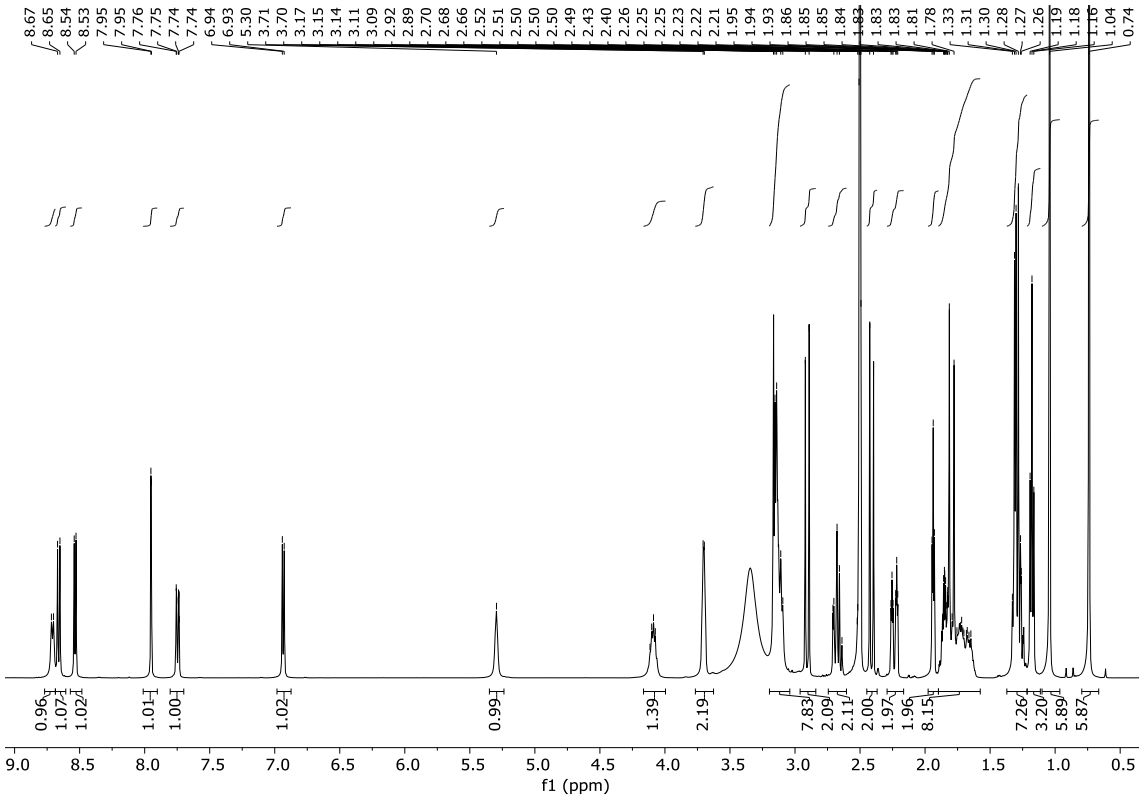


Figure S14. $^{1}H$ NMR spectrum of $[HCQH_2][CampSO_3]_2$ in DMSO-$d_6$.

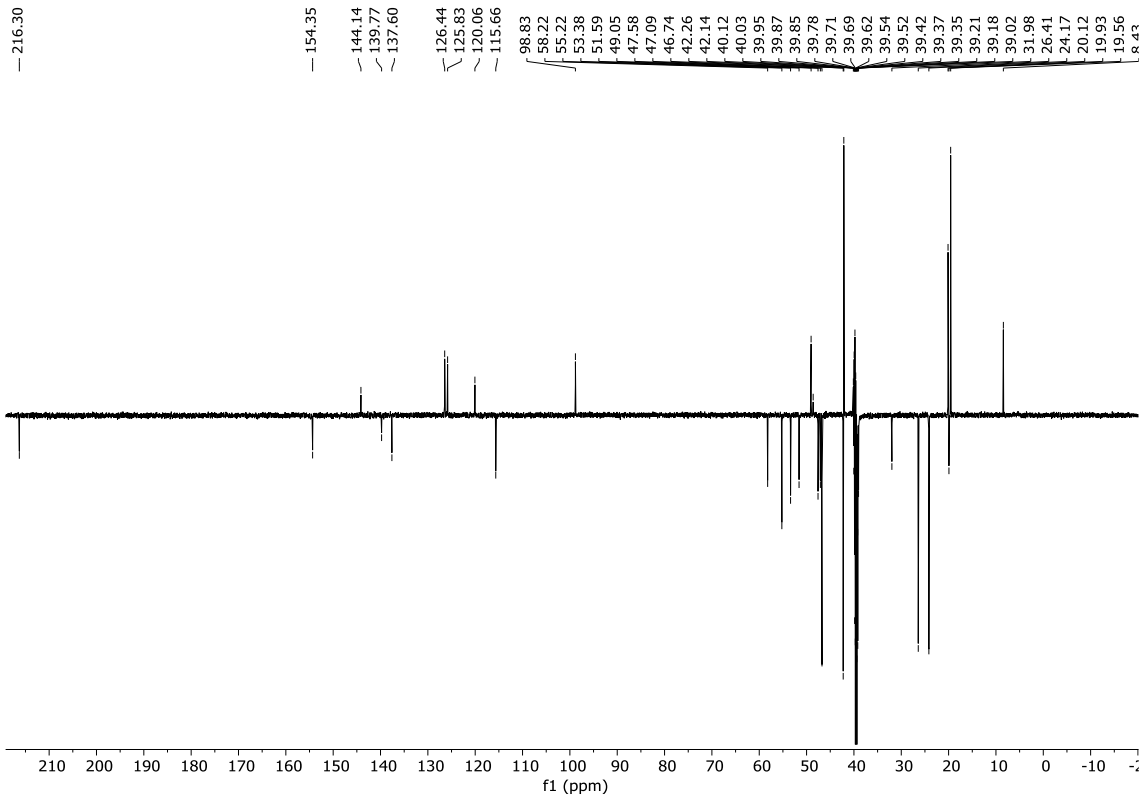


Figure S15. $^{13}C$ APT NMR spectrum of $[HCQH_2][CampSO_3]_2$ in DMSO-$d_6$.

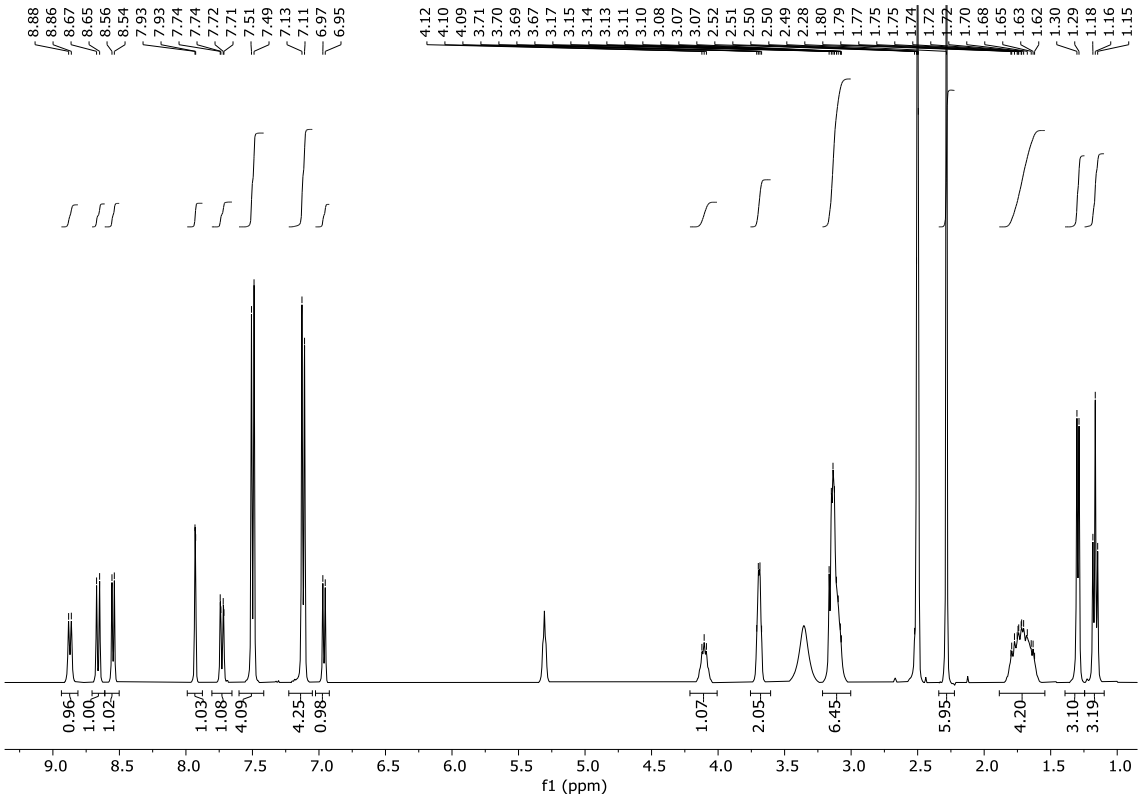


Figure S16. $^{1}$H NMR spectrum of [HCQH$_2$][*p*-TolSO$_3$]$_2$ in DMSO-*d*$_6$.

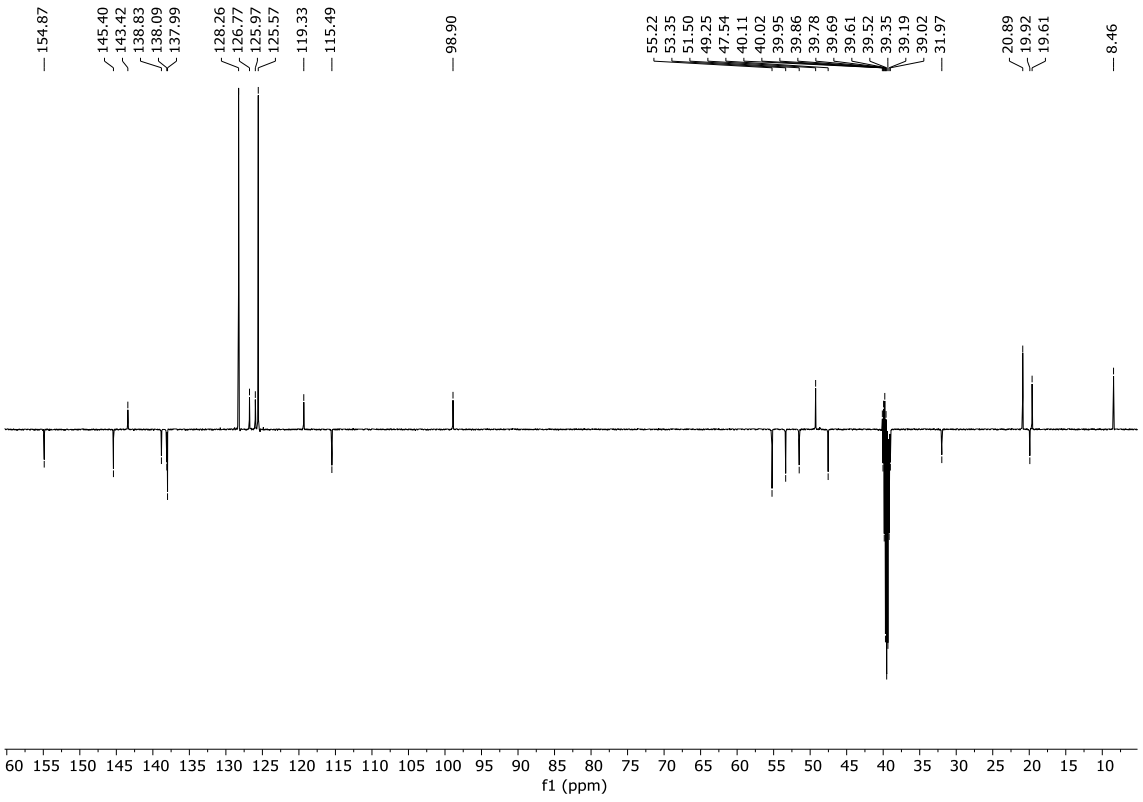


Figure S17. $^{13}$C APT NMR spectrum of [HCQH$_2$][*p*-TolSO$_3$]$_2$ in DMSO-*d*$_6$.

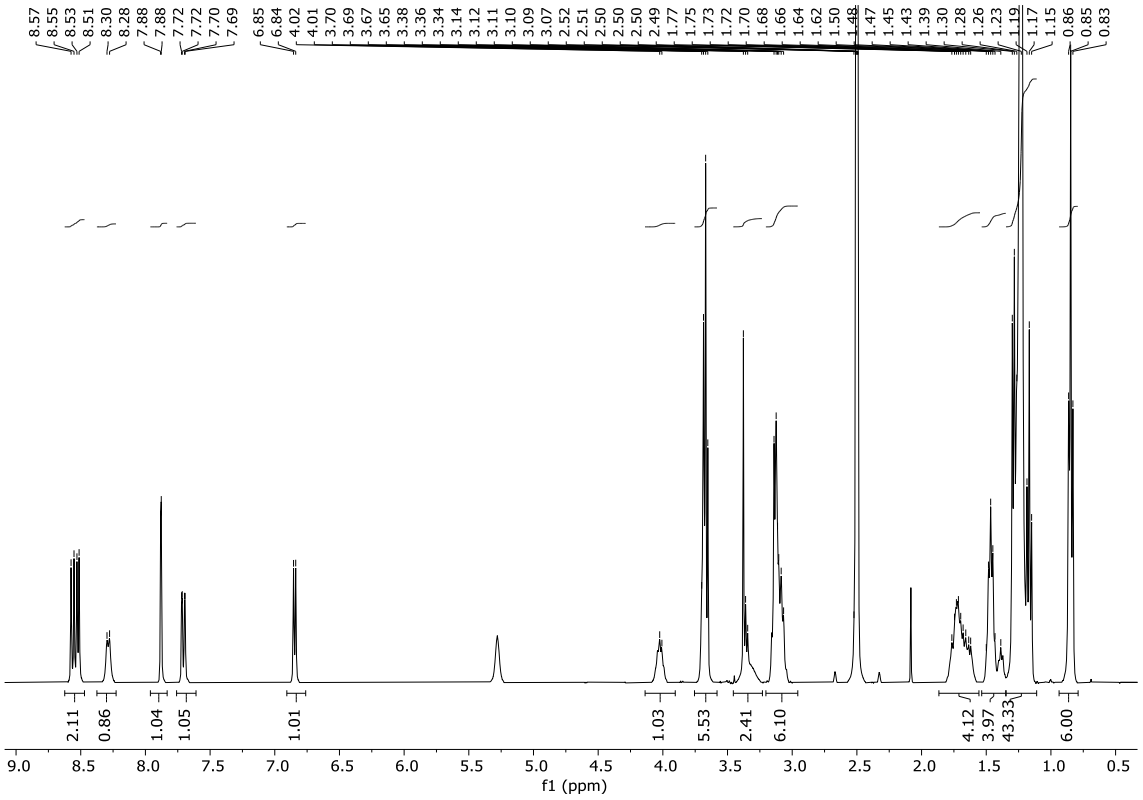


Figure S18. $^{1}H$ NMR spectrum of $[HCQH_2][C_{12}SO_4]_2$ in DMSO-$d_6$.

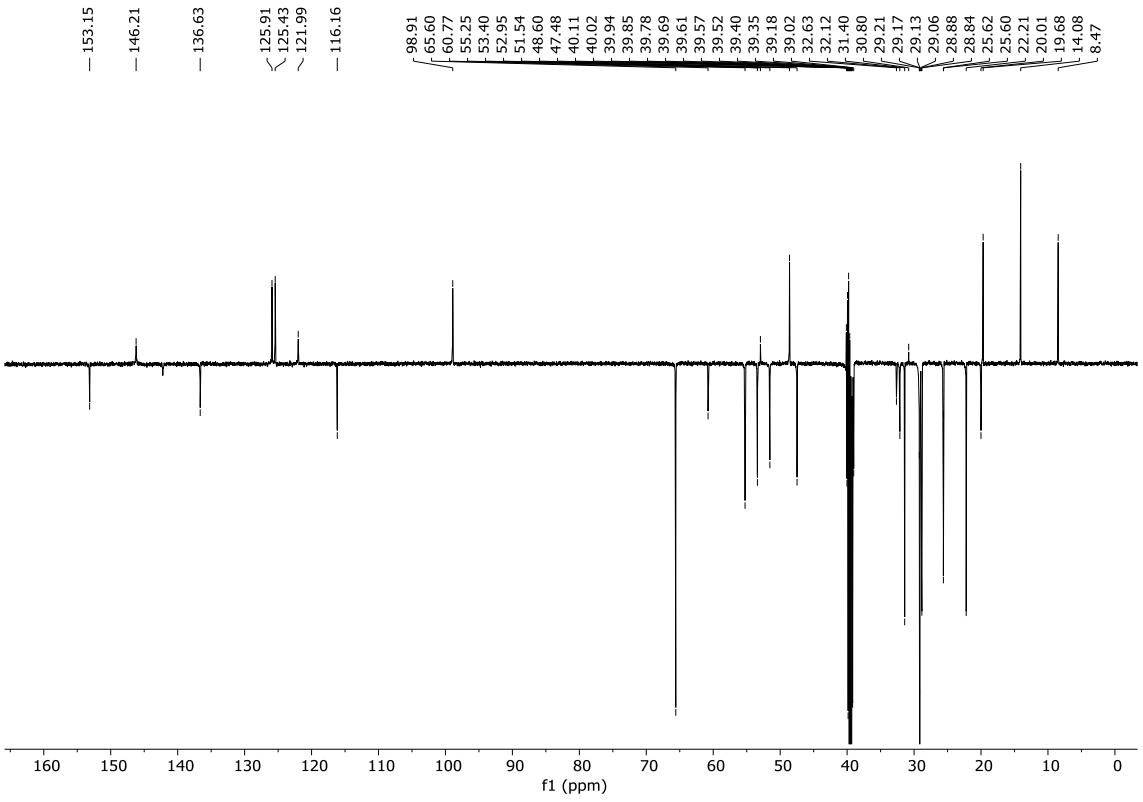


Figure S19. $^{13}C$ APT NMR spectrum of $[HCQH_2][C_{12}SO_4]_2$ in DMSO-$d_6$.

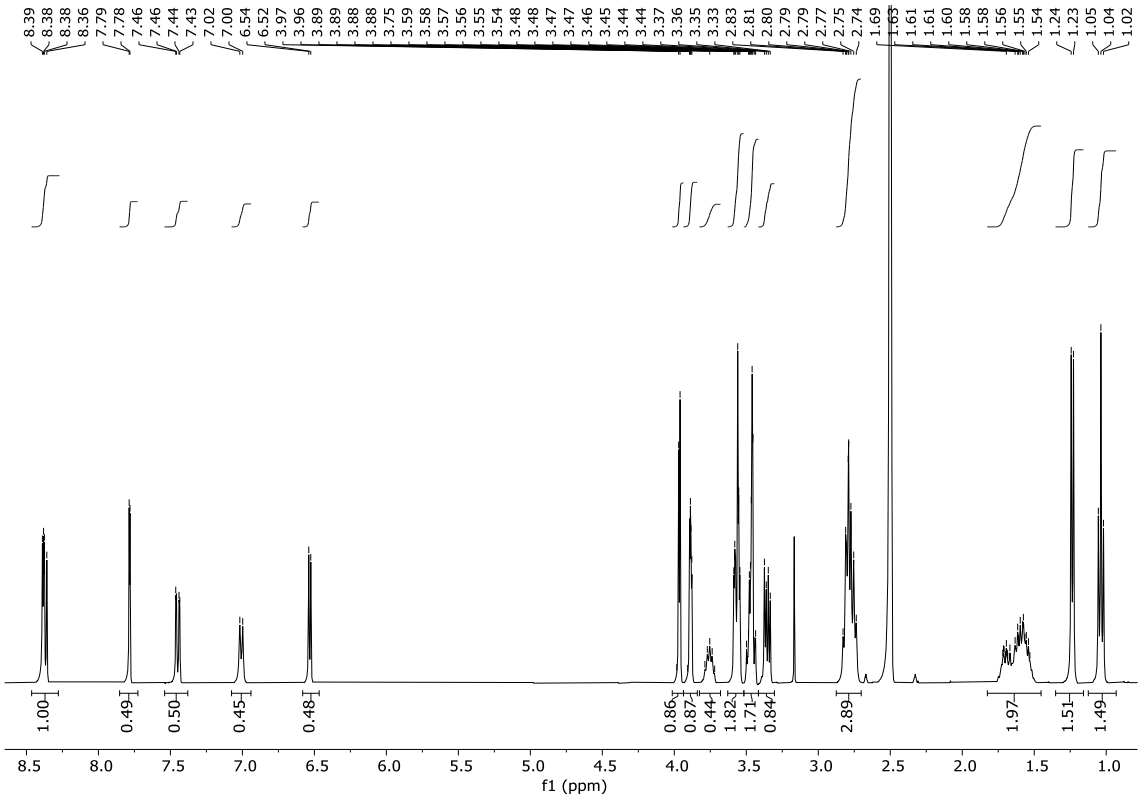


Figure S20. $^{1}$H NMR spectrum of [HCQH$_2$][GlcCOO]$_2$ in DMSO-*d*$_6$.

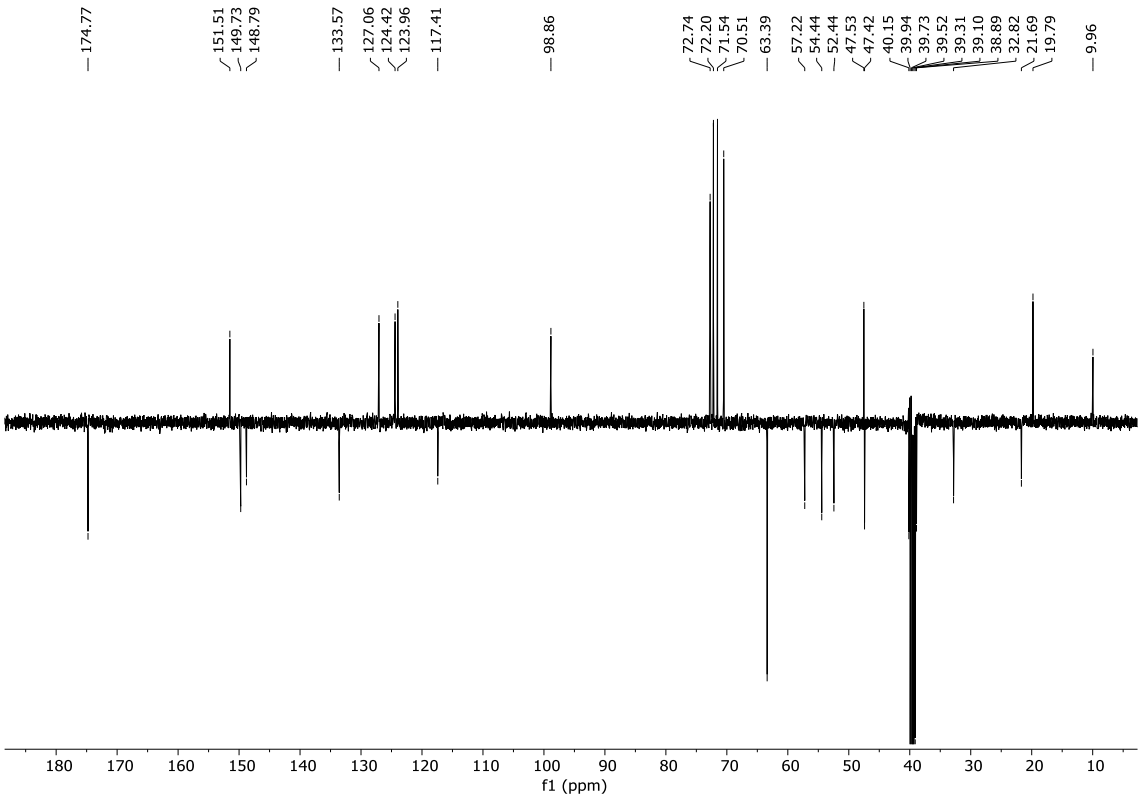


Figure S21. $^{13}$C APT NMR spectrum of [HCQH$_2$][GlcCOO]$_2$ in DMSO-*d*$_6$.

*HRMS spectra*

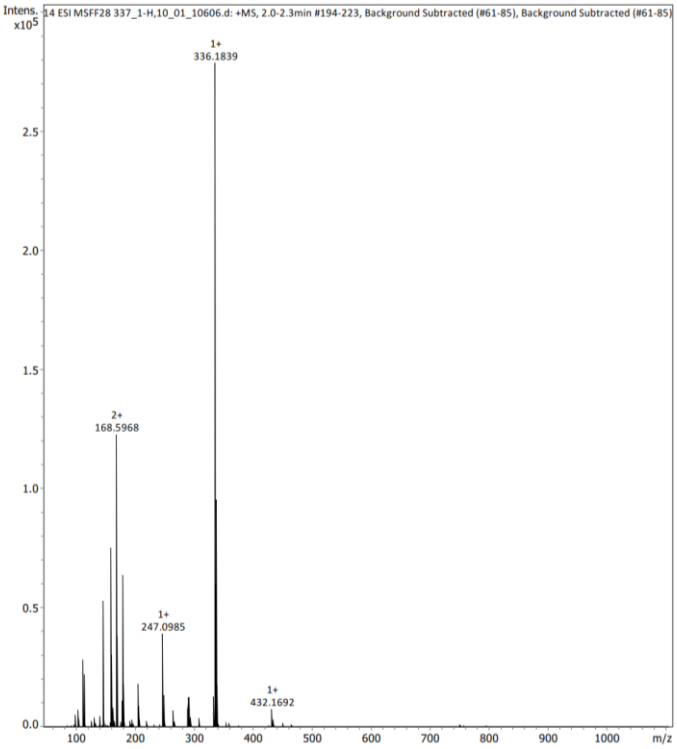


Figure S22. ESI-TOF mass spectra in positive mode of $[HCQH_2][C_1SO_3]_2$.

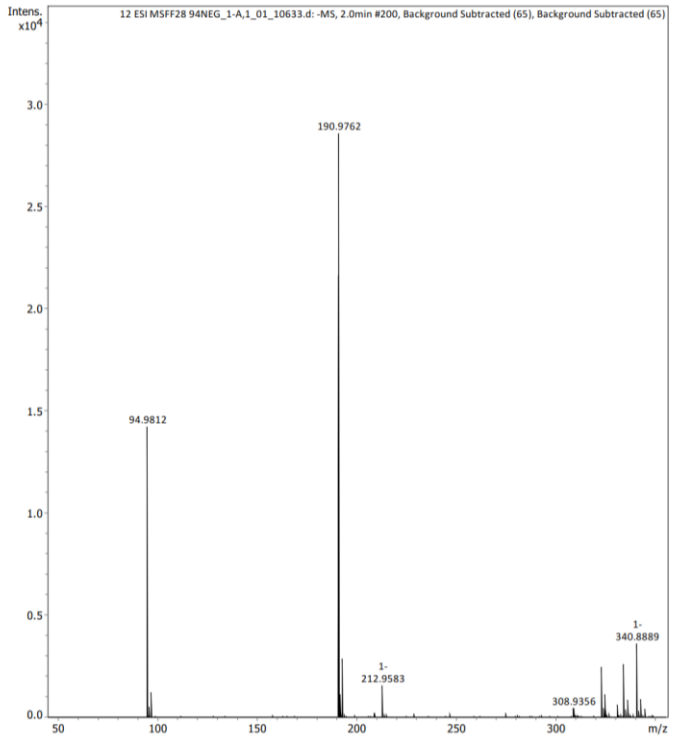


Figure S23. ESI-TOF mass spectra in negative mode of $[HCQH_2][C_1SO_3]_2$.

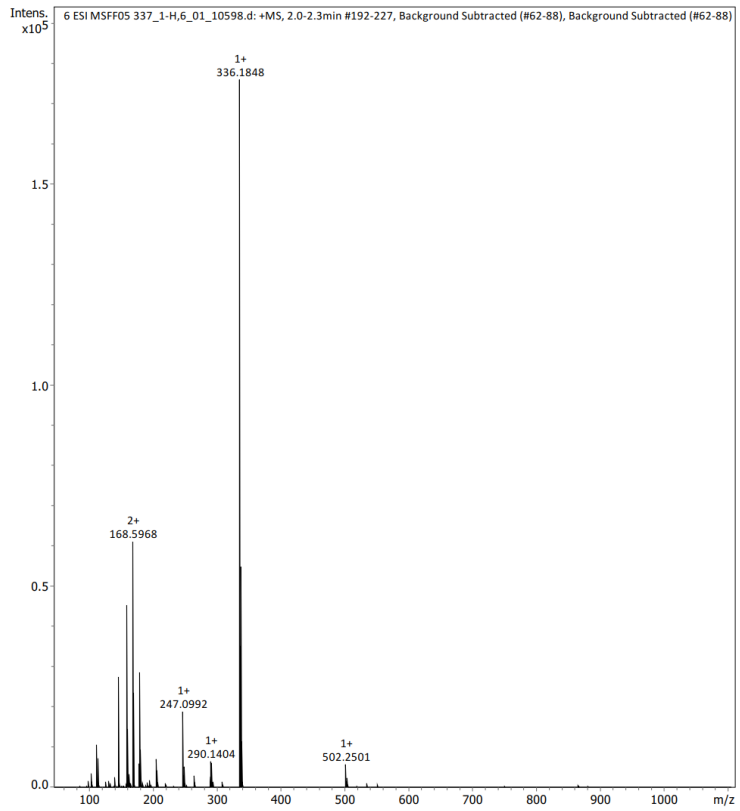


Figure S24. ESI-TOF mass spectra in positive mode of $[HCQH_2][C_6SO_3]_2$.

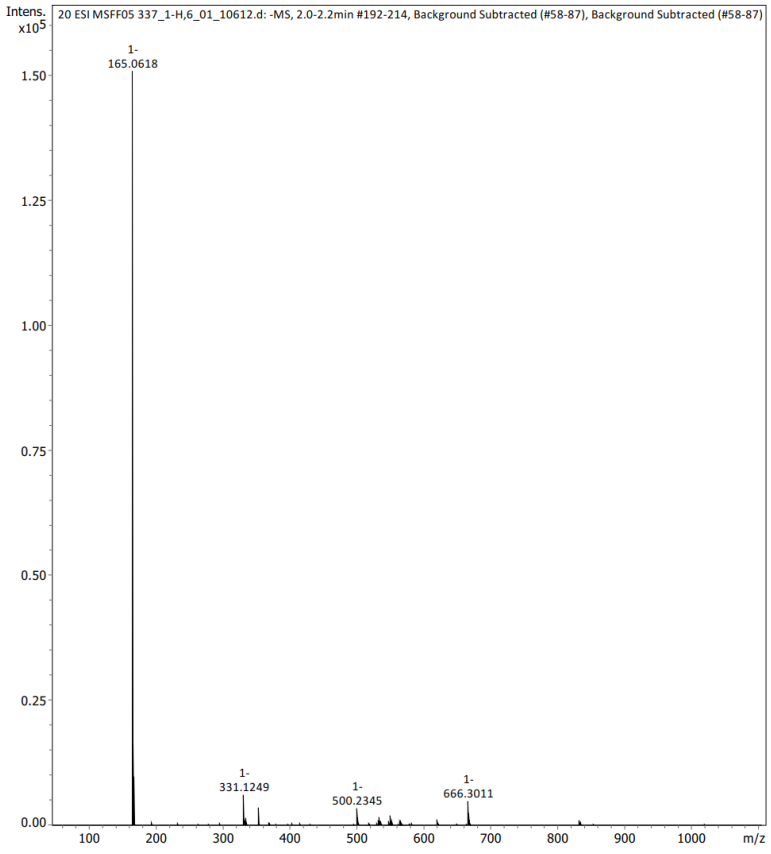


Figure S25. ESI-TOF mass spectra in negative mode of $[HCQH_2][C_6SO_3]_2$.

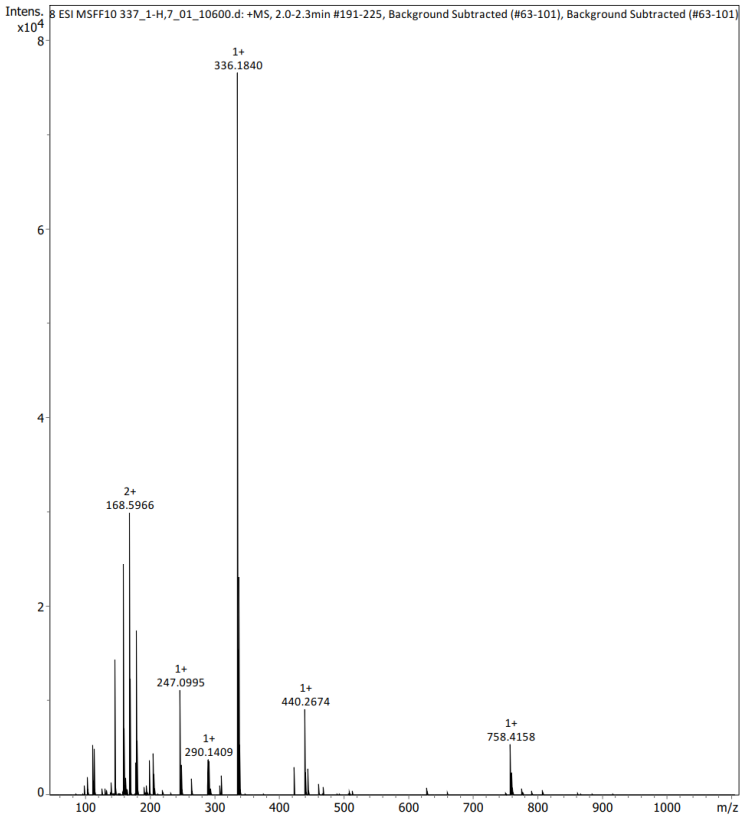


Figure S26. ESI-TOF mass spectra in positive mode of [HCQH$_2$][DocSO$_3$]$_2$.

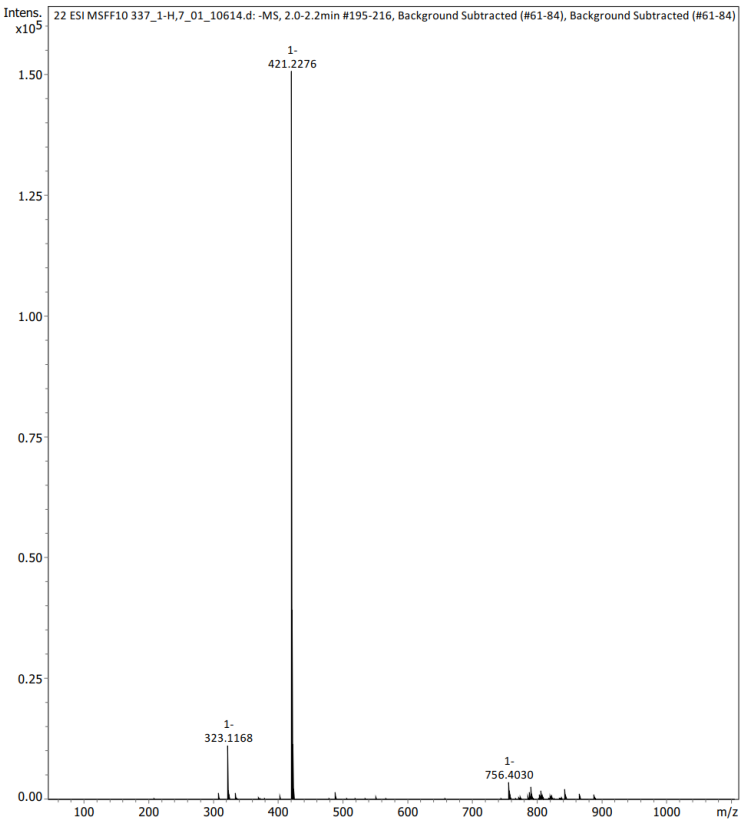


Figure S27. ESI-TOF mass spectra in negative mode of [HCQH$_2$][DocSO$_3$]$_2$.

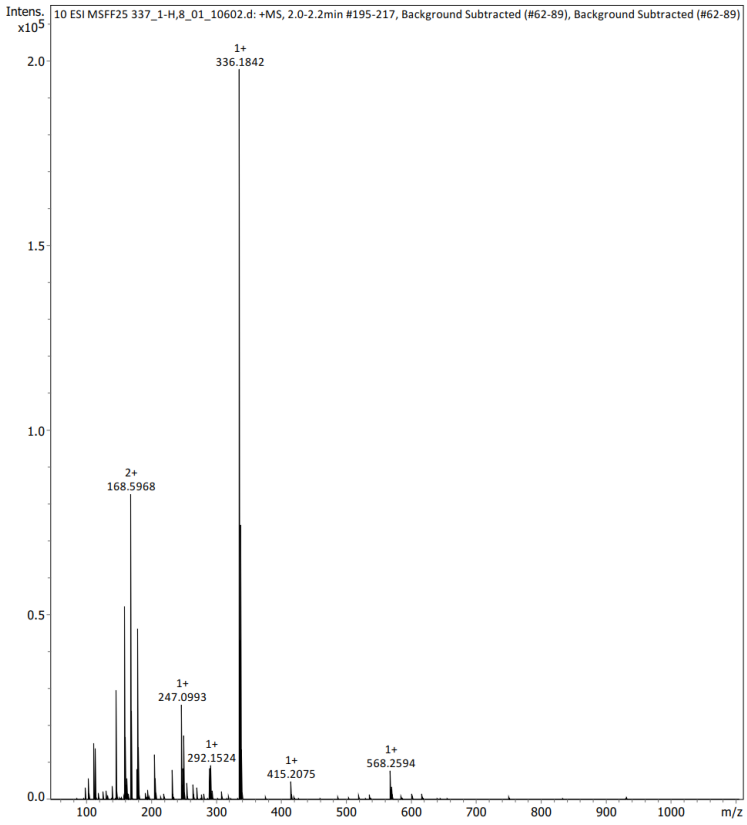


Figure S28. ESI-TOF mass spectra in positive mode of $[HCQH_2][CampSO_3]_2$.

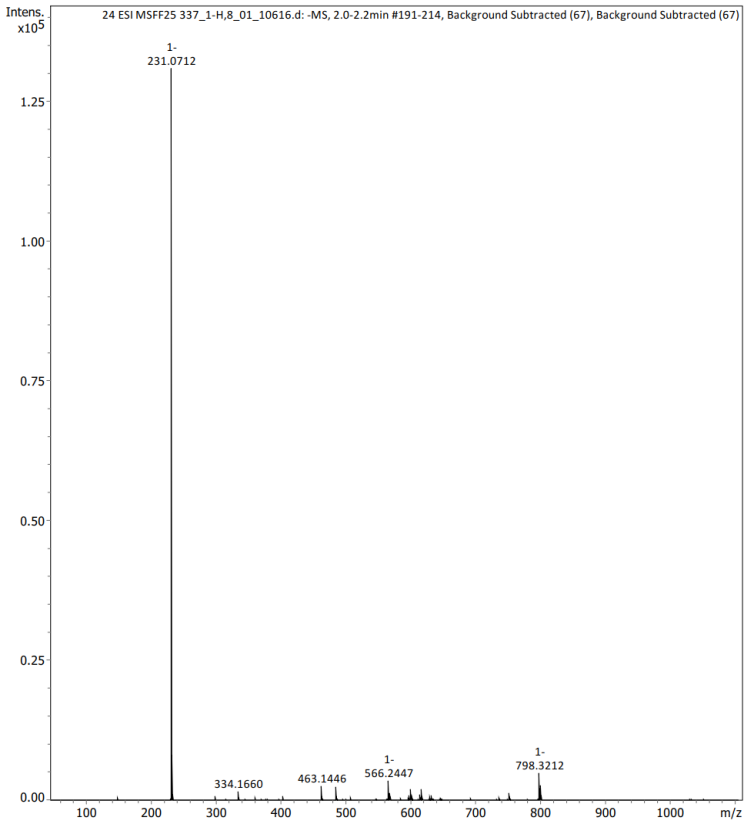


Figure S29. ESI-TOF mass spectra in negative mode of $[HCQH_2][CampSO_3]_2$.

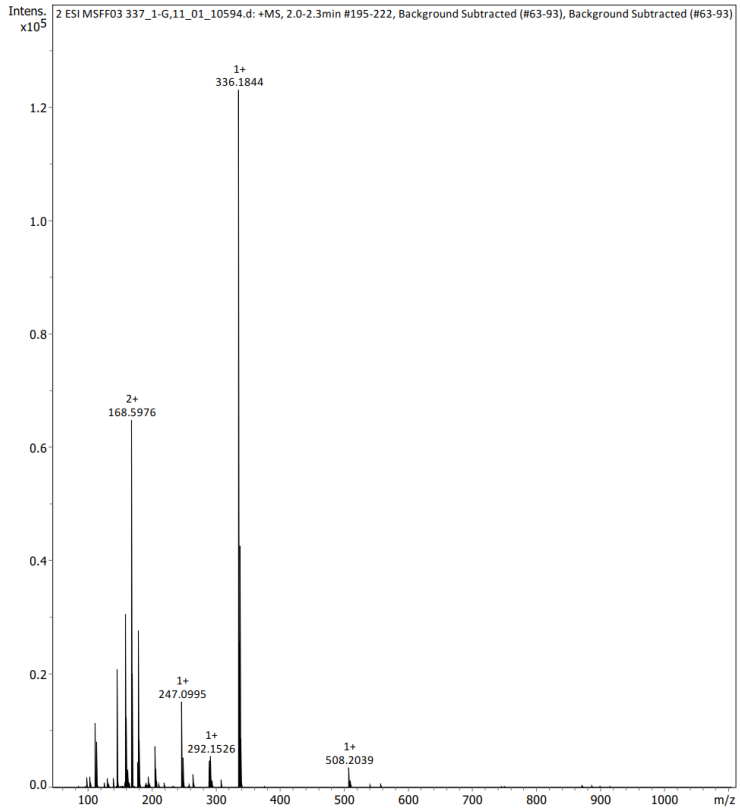


Figure S30. ESI-TOF mass spectra in positive mode of [HCQH$_2$][*p*-TolSO$_3$]$_2$.

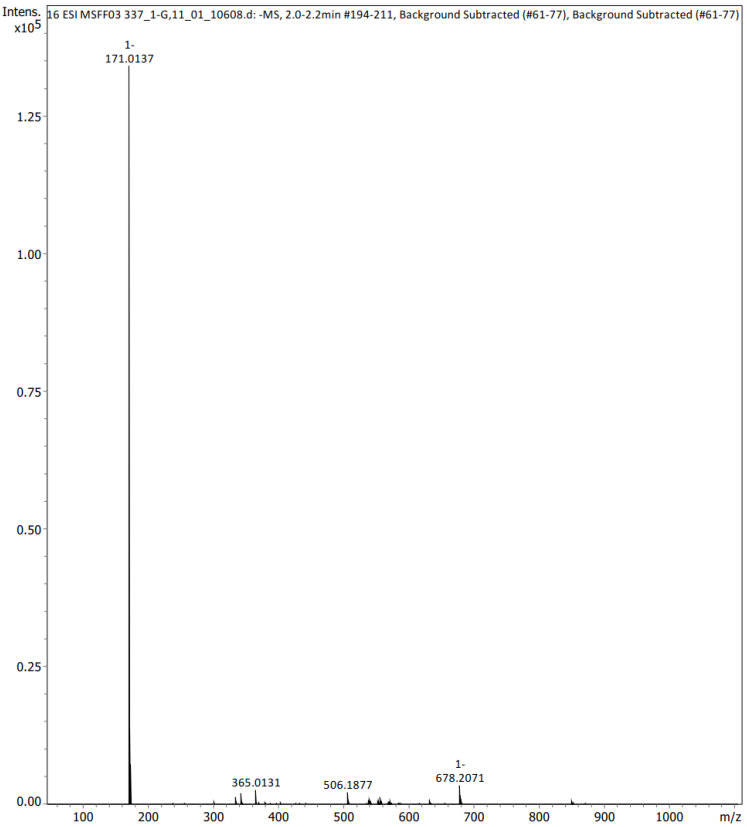


Figure S31. ESI-TOF mass spectra in negative mode of [HCQH$_2$][*p*-TolSO$_3$]$_2$.

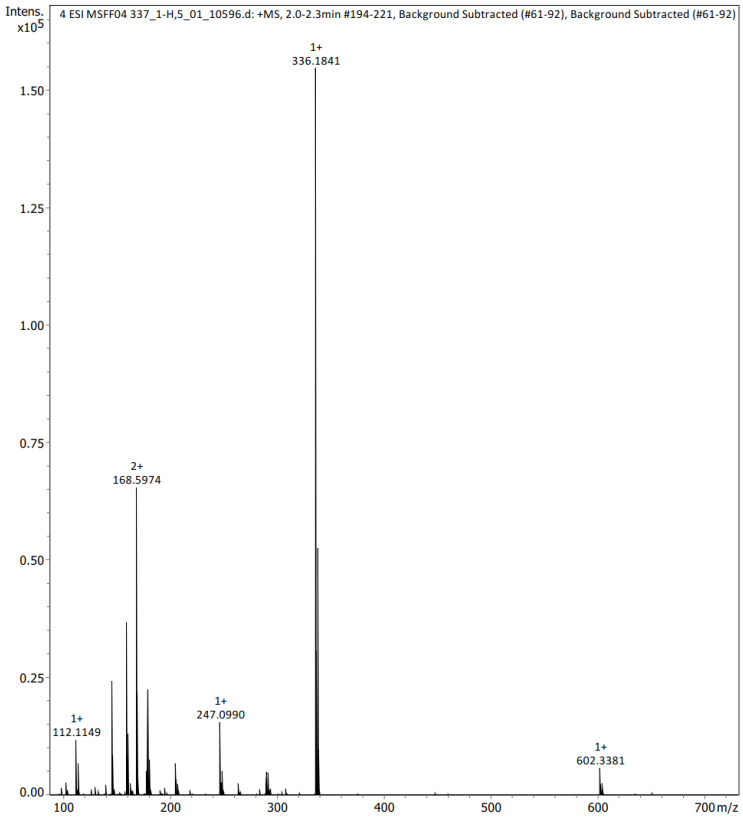


Figure S32. ESI-TOF mass spectra in positive mode of $[HCQH_2][C_{12}SO_4]_2$.

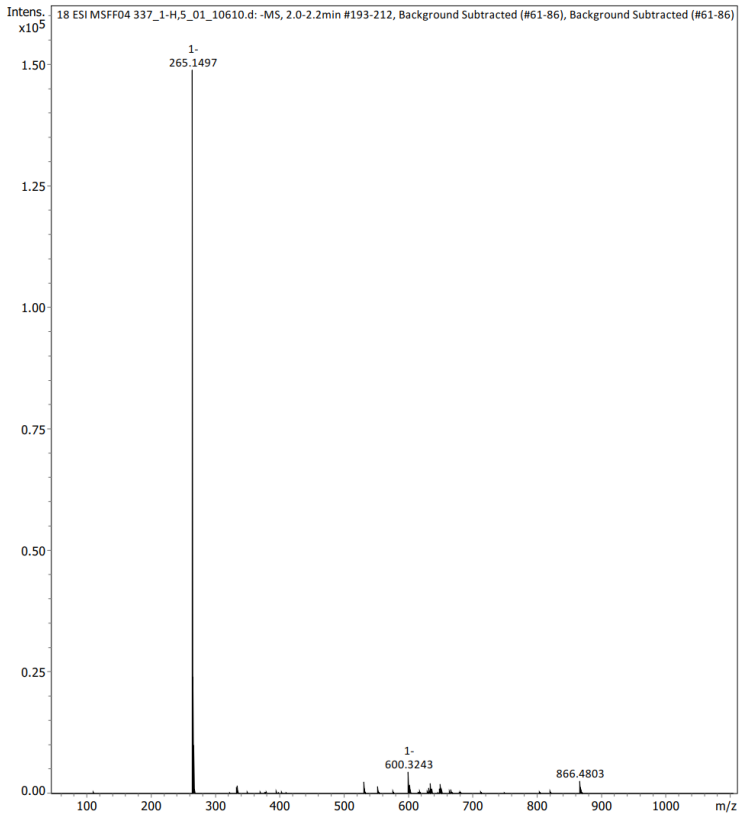


Figure S33. ESI-TOF mass spectra in negative mode of $[HCQH_2][C_{12}SO_4]_2$.

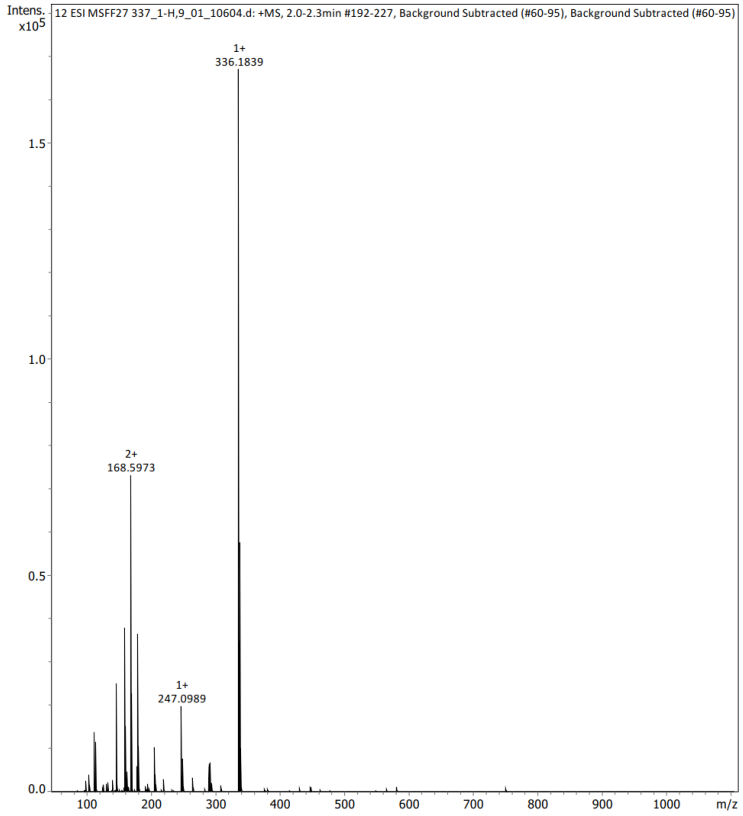


Figure S34. ESI-TOF mass spectra in positive mode of $[HCQH_2][GlcCOO]_2$.

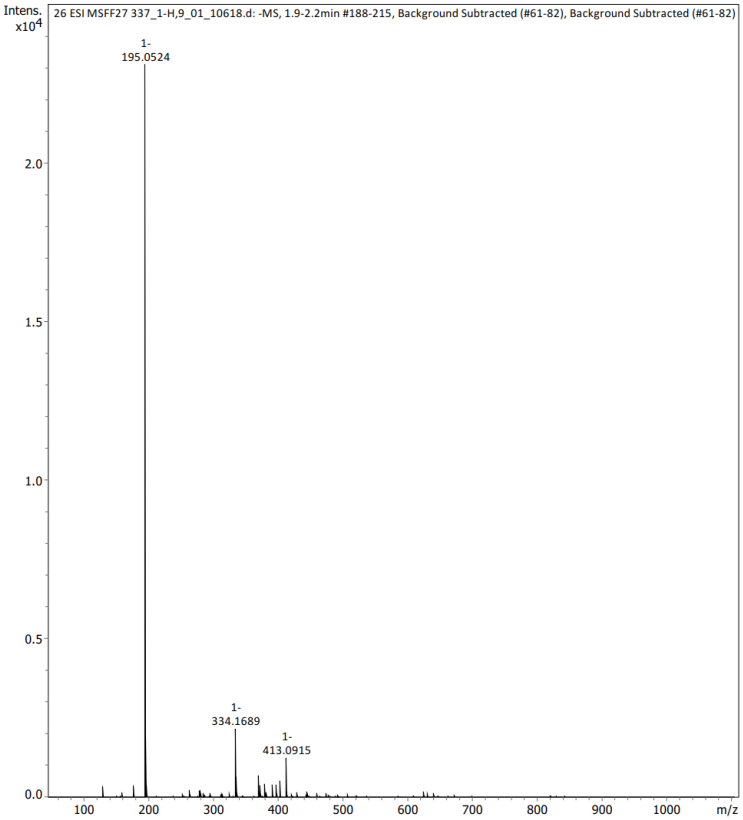


Figure S35. ESI-TOF mass spectra in negative mode of $[HCQH_2][GlcCOO]_2$.

Table S1. Experimental and calculated *m*/*z* values and corresponding errors (ppm) for the $[M+1]^+$ and $[M+2]^{2+}$ ions in positive mode of ESI-TOF for each HCQ-IL.

| | **Exp. *m*/*z* $[M+1]^+$** | **Calc. *m*/*z* $[M+1]^+$** | **error /ppm** | **Exp. *m*/*z* $[M+2]^{2+}$** | **Calc. *m*/*z* $[M+2]^{2+}$** | **error /ppm** |
|---|---|---|---|---|---|---|
| $[HCQH_2][C_1SO_3]_2$ | 336.1839 | 336.1837 | -0.59 | 168.5968 | 168.5955 | -7.71 |
| $[HCQH_2][C_6SO_3]_2$ | 336.1848 | 336.1837 | -3.27 | 168.5968 | 168.5955 | -7.71 |
| $[HCQH_2][DocSO_3]_2$ | 336.1840 | 336.1837 | -0.89 | 168.5966 | 168.5955 | -6.52 |
| $[HCQH_2][CampSO_3]_2$ | 336.1842 | 336.1837 | -1.49 | 168.5968 | 168.5955 | -7.71 |
| $[HCQH_2][p\text{-}TolSO_3]_2$ | 336.1844 | 336.1837 | -2.08 | 168.5976 | 168.5955 | -12.46 |
| $[HCQH_2][C_{12}SO_4]_2$ | 336.1841 | 336.1837 | -1.19 | 168.5974 | 168.5955 | -11.27 |
| $[HCQH_2][GlcCOO]_2$ | 336.1839 | 336.1837 | -0.59 | 168.5973 | 168.5955 | -10.68 |

Table S2. Experimental and calculated *m*/*z* values and corresponding errors (ppm) for the $[M-1]^-$ ion in negative mode of ESI-TOF for each HCQ-IL.

| | **Exp. *m*/*z* $[M-1]^-$** | **Calc. *m*/*z* $[M-1]^-$** | **error /ppm** |
|---|---|---|---|
| $[HCQH_2][C_1SO_3]_2$ | 94.9808 | 94.9812 | 4.21 |
| $[HCQH_2][C_6SO_3]_2$ | 165.0618 | 165.0590 | -16.96 |
| $[HCQH_2][DocSO_3]_2$ | 421.2276 | 421.2265 | -2.61 |
| $[HCQH_2][CampSO_3]_2$ | 231.0696 | 231.0712 | 6.92 |
| $[HCQH_2][p\text{-}TolSO_3]_2$ | 171.0137 | 171.0121 | -9.36 |
| $[HCQH_2][C_{12}SO_4]_2$ | 265.1497 | 265.1479 | -6.79 |
| $[HCQH_2][GlcCOO]_2$ | 195.0510 | 195.0524 | 7.18 |

*DSC thermograms*

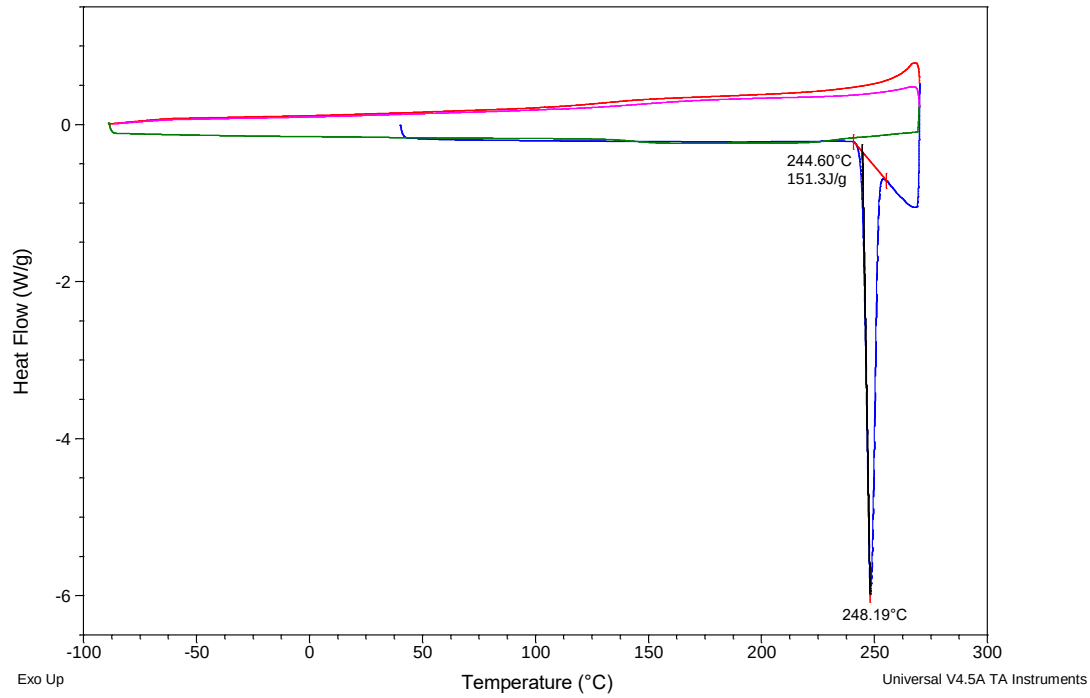


Figure S36. DSC thermogram of $[HCQH_2][SO_4]$.

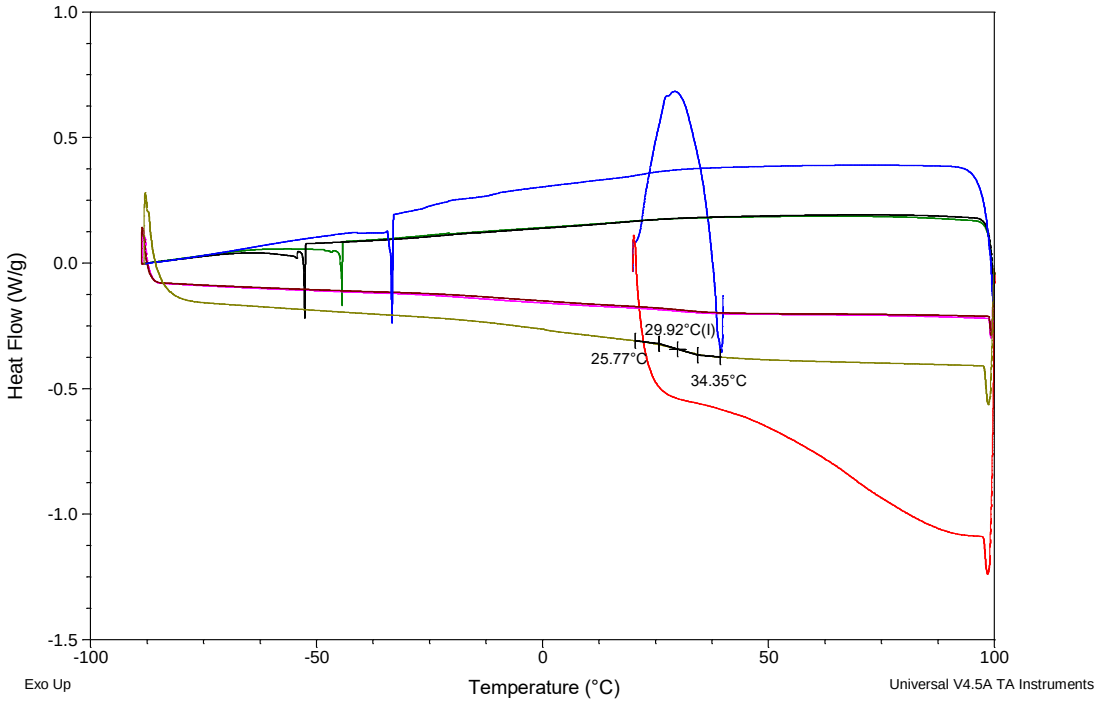


Figure S37. DSC thermogram of $[HCQH_2][C_1SO_3]_2$.

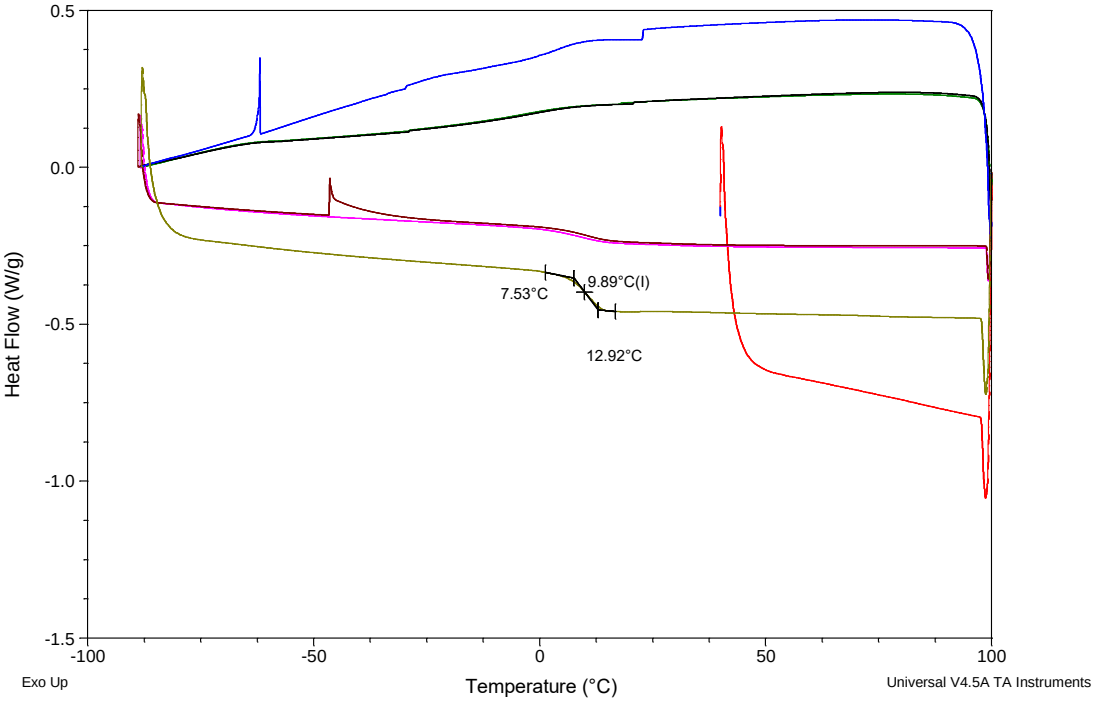


Figure S38. DSC thermogram of $[HCQH_2][C_6SO_3]_2$.

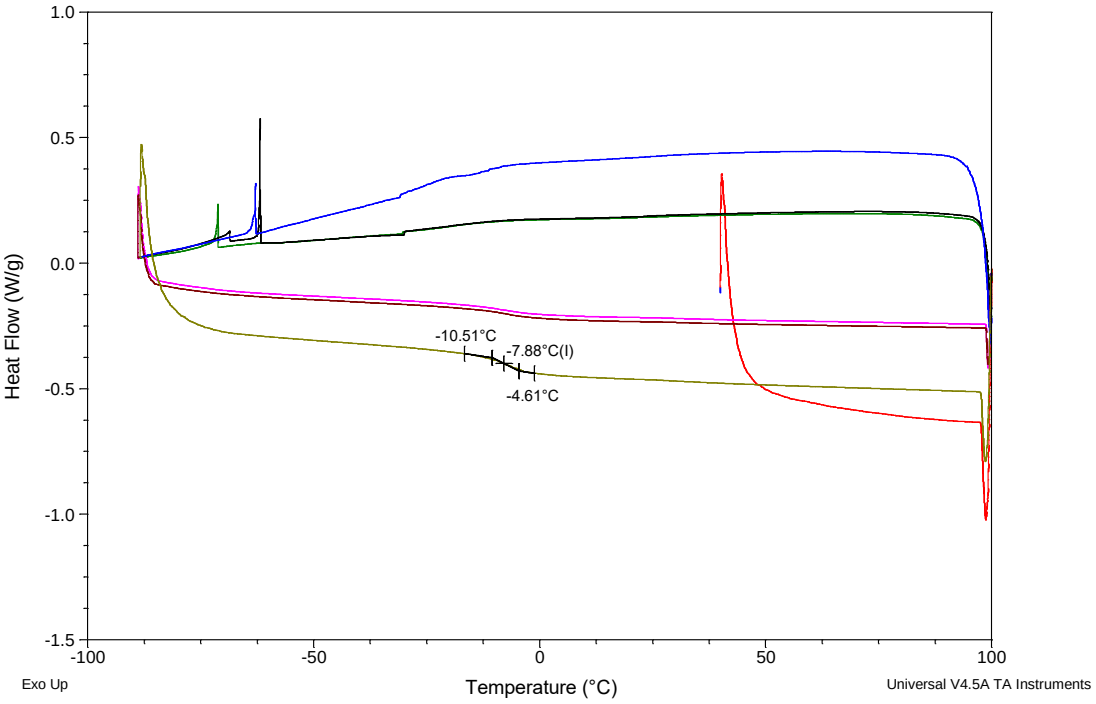


Figure S39. DSC thermogram of $[HCQH_2][DocSO_3]_2$.

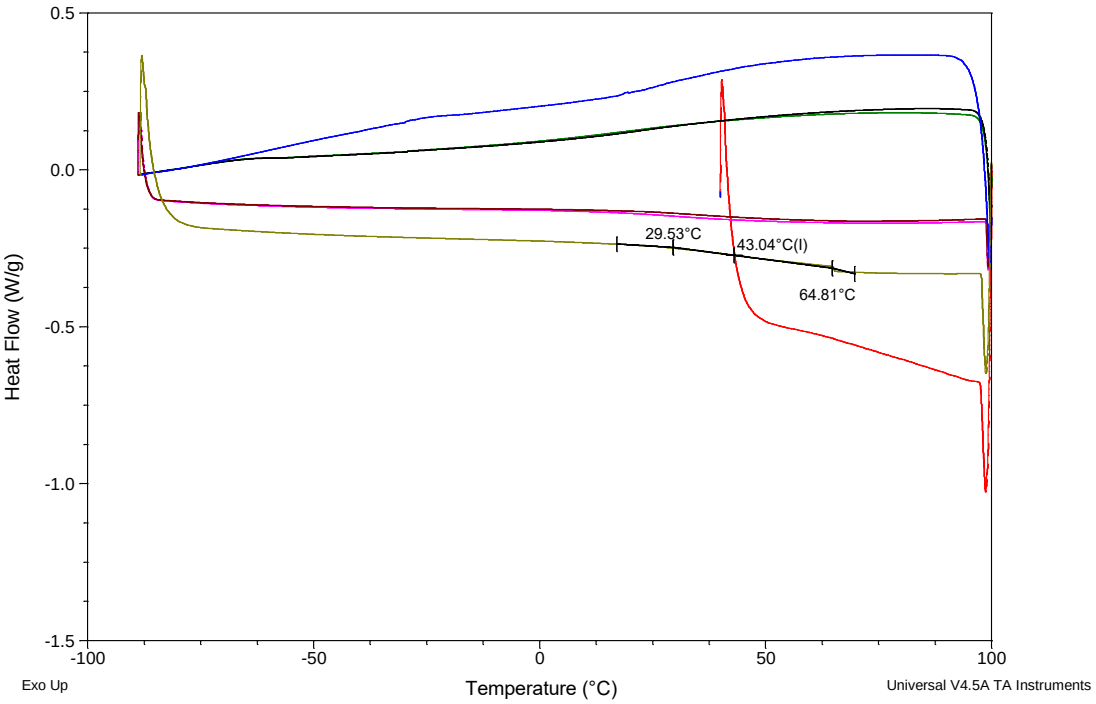


Figure S40. DSC thermogram of $[HCQH_2][CampSO_3]_2$.

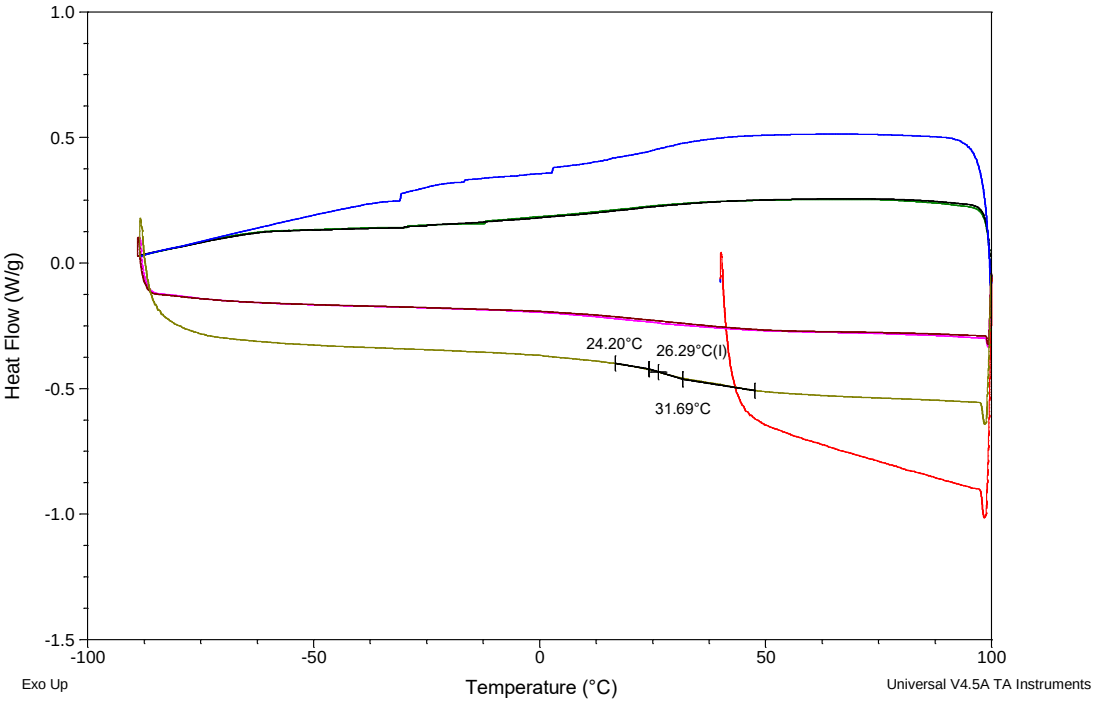


Figure S41. DSC thermogram of $[HCQH_2][p\text{-}TolSO_3]_2$.

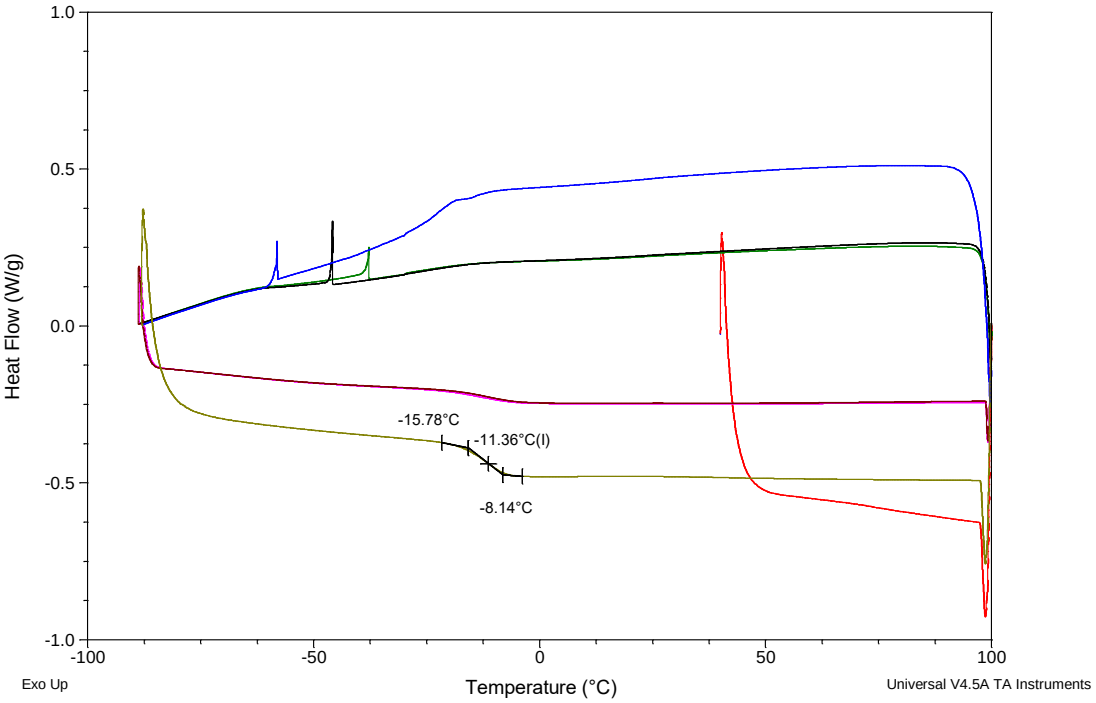


Figure S42. DSC thermogram of $[HCQH_2][C_{12}SO_4]_2$.

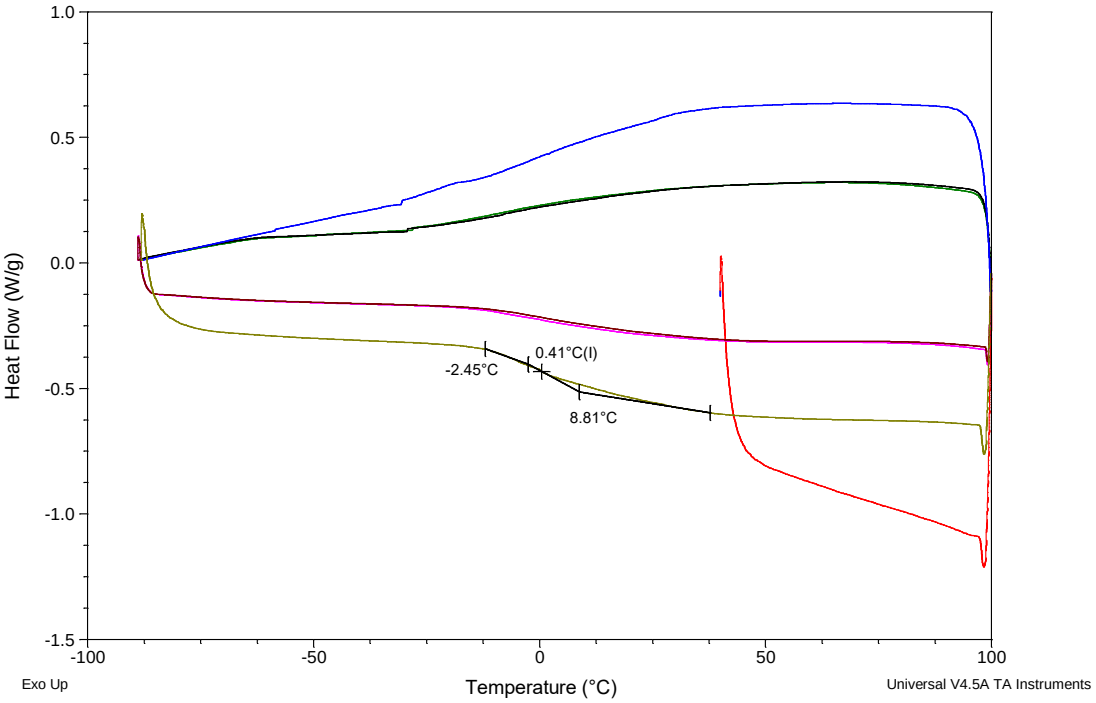


Figure S43. DSC thermogram of $[HCQH_2][GlcCOO]_2$.

*Critical micelle concentrations*

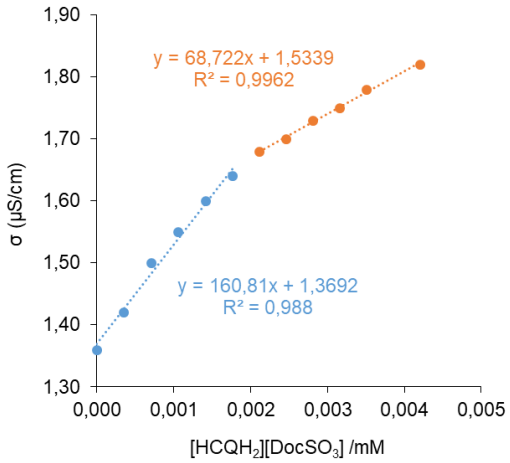


Figure S44. Plot of conductivity *vs* concentration of $[HCQH_2][DocSO_3]_2$ (**5**).

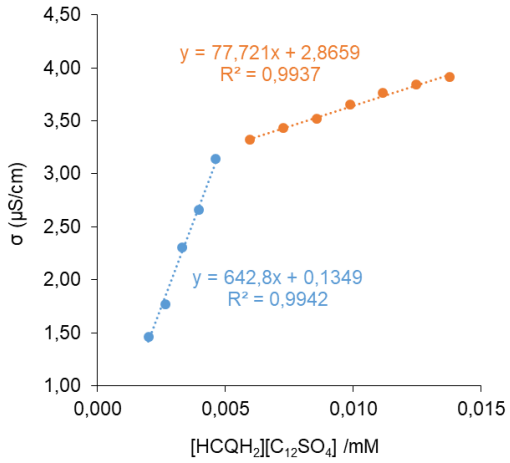


Figure S45. Plot of conductivity *vs* concentration of $[HCQH_2][C_{12}SO_4]_2$ (**8**).